# Measurement of the diffractive structure function in deep inelastic scattering at HERA

ZEUS Collaboration

## Abstract

This paper presents an analysis of the inclusive properties of diffractive deep inelastic scattering events produced in $ep$ interactions at HERA. The events are characterised by a rapidity gap between the outgoing proton system and the remaining hadronic system. Inclusive distributions are presented and compared with Monte Carlo models for diffractive processes. The data are consistent with models where the pomeron structure function has a hard and a soft contribution. The diffractive structure function is measured as a function of $x_{I\!P}$, the momentum fraction lost by the proton, of $\beta$, the momentum fraction of the struck quark with respect to $x_{I\!P}$, and of $Q^2$. The $x_{I\!P}$ dependence is consistent with the form $(1/x_{I\!P})^a$ where $a = 1.30 \pm 0.08 \ (stat) \ ^{+ \ 0.08}_{- \ 0.14} \ (sys)$ in all bins of $\beta$ and $Q^2$. In the measured $Q^2$ range, the diffractive structure function approximately scales with $Q^2$ at fixed $\beta$. In an Ingelman-Schlein type model, where commonly used pomeron flux factor normalisations are assumed, it is found that the quarks within the pomeron do not saturate the momentum sum rule.

# The ZEUS Collaboration

M. Derrick, D. Krakauer, S. Magill, D. Mikunas, B. Musgrave, J. Repond, R. Stanek, R.L. Talaga, H. Zhang
*Argonne National Laboratory, Argonne, IL, USA [p]*

R. Ayad[1], G. Bari, M. Basile, L. Bellagamba, D. Boscherini, A. Bruni, G. Bruni, P. Bruni, G. Cara Romeo,
G. Castellini[2], M. Chiarini, L. Cifarelli[3], F. Cindolo, A. Contin, M. Corradi, I. Gialas[4], P. Giusti, G. Iacobucci,
G. Laurenti, G. Levi, A. Margotti, T. Massam, R. Nania, C. Nemoz,
F. Palmonari, A. Polini, G. Sartorelli, R. Timellini, Y. Zamora Garcia[1], A. Zichichi
*University and INFN Bologna, Bologna, Italy [f]*

A. Bargende[5], J. Crittenden, K. Desch, B. Diekmann[6], T. Doeker, M. Eckert, L. Feld, A. Frey, M. Geerts,
G. Geitz[7], M. Grothe, H. Hartmann, K. Heinloth, E. Hilger, H.-P. Jakob, U.F. Katz,
S.M. Mari[4], A. Mass[8], S. Mengel, J. Mollen, E. Paul, Ch. Rembser, D. Schramm, J. Stamm,
R. Wedemeyer
*Physikalisches Institut der Universität Bonn, Bonn, Federal Republic of Germany [c]*

S. Campbell-Robson, A. Cassidy, N. Dyce, B. Foster, S. George, R. Gilmore, G.P. Heath, H.F. Heath, T.J. Llewellyn,
C.J.S. Morgado, D.J.P. Norman, J.A. O'Mara, R.J. Tapper, S.S. Wilson, R. Yoshida
*H.H. Wills Physics Laboratory, University of Bristol, Bristol, U.K. [o]*

R.R. Rau
*Brookhaven National Laboratory, Upton, L.I., USA [p]*

M. Arneodo[9], M. Capua, A. Garfagnini, L. Iannotti, M. Schioppa, G. Susinno
*Calabria University, Physics Dept.and INFN, Cosenza, Italy [f]*

A. Bernstein, A. Caldwell, N. Cartiglia, J.A. Parsons, S. Ritz[10], F. Sciulli, P.B. Straub, L. Wai, S. Yang, Q. Zhu
*Columbia University, Nevis Labs., Irvington on Hudson, N.Y., USA [q]*

P. Borzemski, J. Chwastowski, A. Eskreys, K. Piotrzkowski, M. Zachara, L. Zawiejski
*Inst. of Nuclear Physics, Cracow, Poland [j]*

L. Adamczyk, B. Bednarek, K. Jeleń, D. Kisielewska, T. Kowalski, E. Rulikowska-Zarębska,
L. Suszycki, J. Zając
*Faculty of Physics and Nuclear Techniques, Academy of Mining and Metallurgy, Cracow, Poland [j]*

A. Kotański, M. Przybycień
*Jagellonian Univ., Dept. of Physics, Cracow, Poland [k]*

L.A.T. Bauerdick, U. Behrens, H. Beier[11], J.K. Bienlein, C. Coldewey, O. Deppe, K. Desler, G. Drews,
M. Flasiński[12], D.J. Gilkinson, C. Glasman, P. Göttlicher, J. Große-Knetter, B. Gutjahr[13], T. Haas, W. Hain,
D. Hasell, H. Heßling, Y. Iga, P. Joos, M. Kasemann, R. Klanner, W. Koch, L. Köpke[14], U. Kötz, H. Kowalski,
J. Labs, A. Ladage, B. Löhr, M. Löwe, J. Lüke, J. Mainusch, O. Mańczak, T. Monteiro[15], J.S.T. Ng, S. Nickel[16],
D. Notz, K. Ohrenberg, M. Roco, M. Rohde, J. Roldán, U. Schneekloth, W. Schulz, F. Selonke, E. Stiliaris[17],
B. Surrow, T. Voß, D. Westphal, G. Wolf, C. Youngman, J.F. Zhou
*Deutsches Elektronen-Synchrotron DESY, Hamburg, Federal Republic of Germany*

H.J. Grabosch, A. Kharchilava, A. Leich, M.C.K. Mattingly, A. Meyer, S. Schlenstedt, N. Wulff
*DESY-Zeuthen, Inst. für Hochenergiephysik, Zeuthen, Federal Republic of Germany*

G. Barbagli, P. Pelfer
*University and INFN, Florence, Italy [f]*

G. Anzivino, G. Maccarrone, S. De Pasquale, L. Votano
*INFN, Laboratori Nazionali di Frascati, Frascati, Italy [f]*

A. Bamberger, S. Eisenhardt, A. Freidhof, S. Söldner-Rembold[18], J. Schroeder[19], T. Trefzger
*Fakultät für Physik der Universität Freiburg i.Br., Freiburg i.Br., Federal Republic of Germany [c]*

N.H. Brook, P.J. Bussey, A.T. Doyle[20], J.I. Fleck[4], D.H. Saxon, M.L. Utley, A.S. Wilson
*Dept. of Physics and Astronomy, University of Glasgow, Glasgow, U.K.* [o]

A. Dannemann, U. Holm, D. Horstmann, T. Neumann, R. Sinkus, K. Wick
*Hamburg University, I. Institute of Exp. Physics, Hamburg, Federal Republic of Germany* [c]

E. Badura[21], B.D. Burow[22], L. Hagge, E. Lohrmann, J. Milewski, M. Nakahata[23], N. Pavel, G. Poelz, W. Schott,
F. Zetsche
*Hamburg University, II. Institute of Exp. Physics, Hamburg, Federal Republic of Germany* [c]

T.C. Bacon, I. Butterworth, E. Gallo, V.L. Harris, B.Y.H. Hung, K.R. Long, D.B. Miller, P.P.O. Morawitz,
A. Prinias, J.K. Sedgbeer, A.F. Whitfield
*Imperial College London, High Energy Nuclear Physics Group, London, U.K.* [o]

U. Mallik, E. McCliment, M.Z. Wang, S.M. Wang, J.T. Wu, Y. Zhang
*University of Iowa, Physics and Astronomy Dept., Iowa City, USA* [p]

P. Cloth, D. Filges
*Forschungszentrum Jülich, Institut für Kernphysik, Jülich, Federal Republic of Germany*

S.H. An, S.M. Hong, S.W. Nam, S.K. Park, M.H. Suh, S.H. Yon
*Korea University, Seoul, Korea* [h]

R. Imlay, S. Kartik, H.-J. Kim, R.R. McNeil, W. Metcalf, V.K. Nadendla
*Louisiana State University, Dept. of Physics and Astronomy, Baton Rouge, LA, USA* [p]

F. Barreiro[24], G. Cases, J.P. Fernandez, R. Graciani, J.M. Hernández, L. Hervás[24], L. Labarga[24], M. Martinez,
J. del Peso, J. Puga, J. Terron, J.F. de Trocóniz
*Univer. Autónoma Madrid, Depto de Física Teoríca, Madrid, Spain* [n]

G.R. Smith
*University of Manitoba, Dept. of Physics, Winnipeg, Manitoba, Canada* [a]

F. Corriveau, D.S. Hanna, J. Hartmann, L.W. Hung, J.N. Lim, C.G. Matthews, P.M. Patel,
L.E. Sinclair, D.G. Stairs, M. St.Laurent, R. Ullmann, G. Zacek
*McGill University, Dept. of Physics, Montréal, Québec, Canada* [a, b]

V. Bashkirov, B.A. Dolgoshein, A. Stifutkin
*Moscow Engineering Physics Institute, Mosocw, Russia* [l]

G.L. Bashindzhagyan, P.F. Ermolov, L.K. Gladilin, Yu.A. Golubkov, V.D. Kobrin, I.A. Korzhavina, V.A. Kuzmin,
O.Yu. Lukina, A.S. Proskuryakov, A.A. Savin, L.M. Shcheglova, A.N. Solomin,
N.P. Zotov
*Moscow State University, Institute of Nuclear Physics, Moscow, Russia* [m]

M. Botje, F. Chlebana, A. Dake, J. Engelen, M. de Kamps, P. Kooijman, A. Kruse, H. Tiecke, W. Verkerke,
M. Vreeswijk, L. Wiggers, E. de Wolf, R. van Woudenberg
*NIKHEF and University of Amsterdam, Netherlands* [i]

D. Acosta, B. Bylsma, L.S. Durkin, K. Honscheid, C. Li, T.Y. Ling, K.W. McLean[25], W.N. Murray, I.H. Park,
T.A. Romanowski[26], R. Seidlein[27]
*Ohio State University, Physics Department, Columbus, Ohio, USA* [p]

D.S. Bailey, A. Byrne[28], R.J. Cashmore, A.M. Cooper-Sarkar, R.C.E. Devenish, N. Harnew,
M. Lancaster, L. Lindemann[4], J.D. McFall, C. Nath, V.A. Noyes, A. Quadt, J.R. Tickner,
H. Uijterwaal, R. Walczak, D.S. Waters, F.F. Wilson, T. Yip
*Department of Physics, University of Oxford, Oxford, U.K.* [o]

G. Abbiendi, A. Bertolin, R. Brugnera, R. Carlin, F. Dal Corso, M. De Giorgi, U. Dosselli,
S. Limentani, M. Morandin, M. Posocco, L. Stanco, R. Stroili, C. Voci
*Dipartimento di Fisica dell' Universita and INFN, Padova, Italy* [f]

J. Bulmahn, J.M. Butterworth, R.G. Feild, B.Y. Oh, J.J. Whitmore[29]
*Pennsylvania State University, Dept. of Physics, University Park, PA, USA [q]*

G. D'Agostini, G. Marini, A. Nigro, E. Tassi
*Dipartimento di Fisica, Univ. 'La Sapienza' and INFN, Rome, Italy [f]*

J.C. Hart, N.A. McCubbin, K. Prytz, T.P. Shah, T.L. Short
*Rutherford Appleton Laboratory, Chilton, Didcot, Oxon, U.K. [o]*

E. Barberis, T. Dubbs, C. Heusch, M. Van Hook, B. Hubbard, W. Lockman, J.T. Rahn, H.F.-W. Sadrozinski, A. Seiden
*University of California, Santa Cruz, CA, USA [p]*

J. Biltzinger, R.J. Seifert, O. Schwarzer, A.H. Walenta, G. Zech
*Fachbereich Physik der Universität-Gesamthochschule Siegen, Federal Republic of Germany [c]*

H. Abramowicz, G. Briskin, S. Dagan[30], A. Levy[31]
*School of Physics,Tel-Aviv University, Tel Aviv, Israel [e]*

T. Hasegawa, M. Hazumi, T. Ishii, M. Kuze, S. Mine, Y. Nagasawa, M. Nakao, I. Suzuki, K. Tokushuku, S. Yamada, Y. Yamazaki
*Institute for Nuclear Study, University of Tokyo, Tokyo, Japan [g]*

M. Chiba, R. Hamatsu, T. Hirose, K. Homma, S. Kitamura, Y. Nakamitsu, K. Yamauchi
*Tokyo Metropolitan University, Dept. of Physics, Tokyo, Japan [g]*

R. Cirio, M. Costa, M.I. Ferrero, L. Lamberti, S. Maselli, C. Peroni, R. Sacchi, A. Solano, A. Staiano
*Universita di Torino, Dipartimento di Fisica Sperimentale and INFN, Torino, Italy [f]*

M. Dardo
*II Faculty of Sciences, Torino University and INFN - Alessandria, Italy [f]*

D.C. Bailey, D. Bandyopadhyay, F. Benard, M. Brkic, M.B. Crombie, D.M. Gingrich[32], G.F. Hartner, K.K. Joo, G.M. Levman, J.F. Martin, R.S. Orr, C.R. Sampson, R.J. Teuscher
*University of Toronto, Dept. of Physics, Toronto, Ont., Canada [a]*

C.D. Catterall, T.W. Jones, P.B. Kaziewicz, J.B. Lane, R.L. Saunders, J. Shulman
*University College London, Physics and Astronomy Dept., London, U.K. [o]*

K. Blankenship, B. Lu, L.W. Mo
*Virginia Polytechnic Inst. and State University, Physics Dept., Blacksburg, VA, USA [q]*

W. Bogusz, K. Charchuła, J. Ciborowski, J. Gajewski, G. Grzelak, M. Kasprzak, M. Krzyżanowski, K. Muchorowski, R.J. Nowak, J.M. Pawlak, T. Tymieniecka, A.K. Wróblewski, J.A. Zakrzewski, A.F. Żarnecki
*Warsaw University, Institute of Experimental Physics, Warsaw, Poland [j]*

M. Adamus
*Institute for Nuclear Studies, Warsaw, Poland [j]*

Y. Eisenberg[30], U. Karshon[30], D. Revel[30], D. Zer-Zion
*Weizmann Institute, Nuclear Physics Dept., Rehovot, Israel [d]*

I. Ali, W.F. Badgett, B. Behrens, S. Dasu, C. Fordham, C. Foudas, A. Goussiou, R.J. Loveless, D.D. Reeder, S. Silverstein, W.H. Smith, A. Vaiciulis, M. Wodarczyk
*University of Wisconsin, Dept. of Physics, Madison, WI, USA [p]*

T. Tsurugai
*Meiji Gakuin University, Faculty of General Education, Yokohama, Japan*

S. Bhadra, M.L. Cardy, C.-P. Fagerstroem, W.R. Frisken, K.M. Furutani, M. Khakzad, W.B. Schmidke
*York University, Dept. of Physics, North York, Ont., Canada [a]*

III

IV

# 1 Introduction

We present an analysis of deep inelastic scattering (DIS) events with a large rapidity gap between the outgoing proton system and the remaining hadronic final state. The general properties of these events indicate that the underlying production mechanism is leading twist and diffractive [1, 2]. Diffractive processes are generally understood to proceed through the exchange of a colourless object with the quantum numbers of the vacuum, generically called the pomeron [3]. The true nature of this exchanged "object" remains unclear.

The analysis of soft hadron-hadron collisions implies that pomeron-exchange can be described by a pomeron-hadron coupling constant and a pomeron-propagator [4]. This led to the proposition of Ingelman and Schlein [5] to treat the pomeron as a quasi-real particle which is emitted by a hadron, described in terms of a parton density and characterised by a structure function $F_2^{I\!P}$ which can be studied in deep inelastic scattering. The assumption of factorisation implies that the pomeron structure is independent of the process of emission. Evidence for a partonic structure of the pomeron was observed by the UA8 collaboration [6] and later by the HERA experiments [2, 7, 8, 9]. These data also gave a first insight into the structure function of the pomeron. The UA8 data show a predominantly hard structure, where on average the partons carry a large fraction of the momentum of the pomeron. However, these data could not distinguish between the quark and the gluon content of the pomeron.

This paper presents a study of the structure of the pomeron in DIS at HERA. We discuss first the variables and cuts which are used to isolate diffractive DIS events. The observed kinematic distributions of the data are compared to Monte Carlo models of diffractive processes in a region where the diffractive contribution dominates. A measurement of the diffractive structure function is presented, integrated over $t$, the square of the momentum transfer at the proton vertex, as a function of $x_{I\!P}$, the momentum fraction lost by the proton, of $\beta$, the momentum fraction of the struck quark with respect to $x_{I\!P}$, and of $Q^2$. The data are used to determine the $x_{I\!P}$ dependence at fixed $\beta$ in order to test factorisation; extract the $\beta$ dependence of the diffractive structure function at fixed $Q^2$; investigate the $Q^2$ dependence of the diffractive structure function at fixed $\beta$, in order to test scale invariance; and, examine the general dependence on $x_{I\!P}$, $\beta$ and $Q^2$ by comparing the data with different models for diffractive dissociation.

# 2 Experimental setup

## 2.1 HERA

This analysis is based on data collected with the ZEUS detector at the electron-proton collider HERA. During 1993, HERA was operated at a proton energy, $E_p$, of 820 GeV and an electron energy, $E_e$, of 26.7 GeV. HERA is designed to run with 210 bunches in each of the electron and proton rings, with an interbunch spacing of 96 ns. For the 1993 data-taking 84 paired bunches were filled for each beam and in addition 10 electron and 6 proton bunches were left unpaired for background studies. Typical total currents were 10 mA for both beams.

## 2.2 The ZEUS detector

Details of the ZEUS detector can be found in [10, 11]. The following is hence restricted to a short description of the components relevant to the present analysis.

Charged particles are tracked by the inner tracking detectors which operate in a magnetic field of 1.43 T provided by a thin superconducting coil. Immediately surrounding the beampipe is the vertex detector (VXD) which consists of 120 radial cells, each with 12 sense wires [12]. Surrounding the VXD is the cylindrical central tracking detector (CTD) which consists of 72 cylindrical drift chamber layers, organised into 9 superlayers [13] (5 axial and 4 small angle stereo layers). In events with charged tracks, using the combined data from both chambers, resolutions of 0.4 cm in $Z$ and 0.1 cm in radius in the $XY$ plane[1] are obtained for the primary vertex reconstruction.

The high resolution uranium-scintillator calorimeter (CAL) [14, 15, 16] consists of three parts, forward (FCAL) covering the pseudorapidity[2] region $4.3 \geq \eta \geq 1.1$, barrel (BCAL) covering the central region $1.1 \geq \eta \geq -0.75$ and rear (RCAL) covering the backward region $-0.75 \geq \eta \geq -3.8$. Holes of $20 \times 20$ cm$^2$ in the centre of FCAL and RCAL are required to accommodate the HERA beam pipe. The resulting solid angle coverage is 99.7% of $4\pi$. The calorimeter is subdivided longitudinally into one electromagnetic (EMC) section and one (RCAL) or two (FCAL and BCAL) hadronic (HAC) sections. The sections are subdivided into cells, each of which is read out by two photomultiplier tubes. The CAL also provides a time resolution of better than 1 ns for energy deposits greater than 4.5 GeV, which is used for background rejection.

The C5 beam monitor, a small lead-scintillator counter assembly around the beam pipe located at $Z = -3.2$ m, has been used to measure the timing and longitudinal structure of the proton and electron bunches, and to reject events from upstream proton-gas interactions. The vetowall detector, consisting of two layers of orthogonal scintillator strips on either side of an 87 cm thick iron wall centred at $Z = -7.3$ m, was also used to tag upstream background events.

The luminosity is measured from the rate observed in the luminosity photon detector of hard bremsstrahlung photons from the Bethe-Heitler process $ep \rightarrow e'p\gamma$. The luminosity detector [17] consists of a photon and an electron lead-scintillator calorimeter. Bremsstrahlung photons emerging from the electron-proton interaction point at angles below 0.5 mrad with respect to the electron beam axis hit the photon calorimeter placed at 107 m distance along the electron beam line. Electrons emitted at scattering angles less than 5 mrad and with energies $0.2E_e < E'_e < 0.9E_e$ are deflected by beam magnets and hit the electron calorimeter placed 35 m from the interaction point.

## 2.3 Trigger conditions

Data were collected with a three level trigger [10]; details of the first (FLT) and second (SLT) level decision for DIS events can be found in previous publications [18].

---

[1]The ZEUS coordinate system is defined as right handed with the $Z$ axis pointing in the proton beam direction, hereafter referred to as forward, the $X$ axis pointing towards the centre of HERA and the $Y$ axis pointing upwards.

[2]The pseudorapidity $\eta$ is defined as $-\ln(\tan\frac{\theta}{2})$, where the polar angle $\theta$ is taken with respect to the proton beam direction and, in this case, refers to the nominal interaction point.

The third level trigger (TLT) rejects beam-gas events using timing and cosmic-ray events by a combination of timing and topology. Finally it passes the accepted events through a set of filters in order to categorise the events. The category of DIS neutral current events is defined by the requirement of an electron candidate in the RCAL or BCAL. A cut was performed on $\delta \equiv \Sigma_i E_i (1 - \cos \theta_i) > 20 \text{GeV} - 2E_\gamma$, where $E_i$ and $\theta_i$ are the energies and polar angles (in this case, with respect to the nominal interaction point) of calorimeter cells and $E_\gamma$ is the energy measured in the photon calorimeter of the luminosity monitor. For events fully contained in the main detector $\delta \simeq 2E_e = 53.4$ GeV, whereas for low-$Q^2$ events the scattered electron escapes through the rear beam pipe and $\delta$ peaks at low values.

# 3   Kinematic variables

The kinematic variables used to describe DIS events

$$e\ (k)\ +\ p\ (P) \to e'\ (k')\ +\ anything$$

are the following: the negative of the squared four-momentum transfer carried by the virtual photon[3]:

$$Q^2 = -q^2 = -(k\ -\ k')^2;$$

the Bjorken variable:

$$x = \frac{Q^2}{2P \cdot q};$$

the variable which describes the energy transfer to the hadronic final state:

$$y = \frac{P \cdot q}{P \cdot k};$$

and the centre-of-mass energy $W$ of the virtual-photon proton $(\gamma^* p)$ system, where:

$$W^2 = (q + P)^2 = \frac{Q^2(1 - x)}{x} + M_p^2$$

with $M_p$ denoting the proton mass.

These variables, only two of which are independent at fixed $ep$ centre-of-mass energy squared $s = (k + P)^2$, can be reconstructed in a variety of ways using combinations of electron and hadronic system energies and angles [19]. The variable $y$, calculated from the electron variables, is given by:

$$y_e = 1 - \frac{E'_e}{E_e} \frac{1 - \cos \theta'_e}{2}$$

where $E'_e$, $\theta'_e$ denote the energy and angle of the scattered electron. Alternatively, $y$ can be estimated from the hadronic system, using the Jacquet-Blondel technique [20]:

$$y_{JB} = \frac{\sum_i E_i(1 - cos\theta_i)}{2 \cdot E_e}$$

---

[3]In the $Q^2$ range used for this analysis, $ep$ interactions are described to sufficient accuracy by the exchange of a virtual photon.

where $E_i$ and $\theta_i$ are the energies and polar angles of calorimeter cells which are associated with the hadronic system.

Studies of the kinematic variables have shown that for this analysis it is advantageous to use the so-called double angle ($DA$) method, in which the angles of the scattered electron and the hadron system are used to determine $x$ and $Q^2$. Quantities determined in this way will be denoted by the subscript $DA$. Formulae to calculate $Q^2_{DA}$, $W_{DA}$, $x_{DA}$ and $y_{DA}$ are given in [19].

In the diffractive DIS process shown in Fig. 1:

$$e\,(k)\,+\,p\,(P) \to e'\,(k')\,+\,p'(P')\,+\,X,$$

the hadronic system $X$ (exclusive of the proton) and the scattered electron $e'$ are detected in the main detector. The proton remnant $p'$ remains undetected. When the system $X$ is fully contained its invariant mass, $M_X$, can be determined from the calorimeter cell information as follows [1]. Denoting the energy, momentum and polar angle of the final hadronic system as $E_H$, $p_H$ and $\theta_H$, respectively; and $\vec{p_i}$ as the vector constructed from the energy $E_i$, polar angle $\theta_i$ and azimuthal angle $\phi_i$ of cell $i$; then:

$$\cos\theta_H = \frac{\sum_i p_{z_i}}{|\sum_i \vec{p_i}|} \tag{1}$$

$$p_H^2 = \frac{Q^2_{DA}(1 - y_{DA})}{\sin^2\theta_H}$$

$$E_H = p_H \cos\theta_H + 2E_e y_{DA}$$

from which $M_X$ is determined by the definition $M_X = \sqrt{E_H^2 - p_H^2}$.

The squared four-momentum transfer at the proton vertex is given by:

$$t = (P - P')^2,$$

whose absolute magnitude is expected to be small compared to $Q^2 + M_X^2$ in diffractive processes for the kinematic region studied here. To describe diffractive deep inelastic scattering, in addition to $x$ and $Q^2$, the following variables are used:

$$x_{I\!P} = \frac{(P - P')\cdot q}{P\cdot q} = \frac{M_X^2 + Q^2 - t}{W^2 + Q^2 - M_p^2} \simeq \frac{M_X^2 + Q^2}{W^2 + Q^2},$$

$$\beta = \frac{Q^2}{2(P - P')\cdot q} = \frac{x}{x_{I\!P}} = \frac{Q^2}{M_X^2 + Q^2 - t} \simeq \frac{Q^2}{M_X^2 + Q^2}.$$

In models where diffraction is described by the exchange of a particle-like pomeron, $x_{I\!P}$ is the momentum fraction of the pomeron in the proton and $\beta$ is the momentum fraction of the struck quark within the pomeron. For the structure of the pomeron in DIS, the variable $\beta$ plays a role analogous to that of Bjorken-$x$ for the structure of the proton.

# 4    Diffractive structure function

For unpolarised beams, the differential cross section for single diffractive dissociation can be described in terms of the diffractive structure function, $F_2^{D(4)}(\beta, Q^2, x_{I\!P}, t)$:

$$\frac{d^4\sigma_{diff}}{d\beta dQ^2 dx_{I\!P} dt} = \frac{2\pi\alpha^2}{\beta Q^4}\left[(1 + (1-y)^2)F_2^{D(4)} - y^2 F_L^{D(4)}\right](1 + \delta_Z)(1 + \delta_r)$$

where $\alpha$ is the electromagnetic coupling constant and the $\delta_i$ denote corrections due to $Z^0$ exchange and due to radiative corrections which are small in the measured range. The contribution of $F_L$ to the diffractive cross section is not known. If such a term were included, the $F_2$ values would become larger at large $y$ values (corresponding to small $x_{I\!P}$ values). The effect of this uncertainty is considered in section 8.1. Note that the function $F_2^{D(4)}(\beta, Q^2, x_{I\!P}, t)$ can be related to that of $\mathcal{F}_2^{D(4)}(x, Q^2, x_{I\!P}, t)$. Integrating $\mathcal{F}_2^{D(4)}$ over $x_{I\!P}$ and $t$ one can directly compare it to the inclusive proton structure function $F_2(x, Q^2)$ [21].

In this analysis, an integral is performed over $t$, corresponding to the (undetected) momentum transfer to the proton system. For this initial measurement we neglect the effect of $F_L$ and the additional contributions noted above, yielding the following expression for $F_2^{D(3)}$, where the cross section is evaluated as a function of $\beta, Q^2$ and $x_{I\!P}$:

$$\frac{d^3\sigma_{diff}}{d\beta dQ^2 dx_{I\!P}} = \frac{2\pi\alpha^2}{\beta Q^4}\left(1 + (1-y)^2\right)F_2^{D(3)}(\beta, Q^2, x_{I\!P}),$$

following the procedure of [22], where the relation $x = \beta x_{I\!P}$ has been used.

# 5    Diffractive models and Monte Carlo simulation

Different approaches exist to model diffractive processes such as that depicted in Fig. 1. In this paper we compare the data with the predictions of the factorisable models of Ingelman and Schlein [5], Donnachie and Landshoff [23] and Capella et al. [24], as well as the non-factorisable model of Nikolaev and Zakharov [25, 26]. We have earlier found that the Monte Carlo implementations [27, 28] of the models described above provide reasonable descriptions of the shape of the energy flow and of the observed fraction of events with one or more jets [2, 45].

In the model of Ingelman and Schlein [5] the proton emits a pomeron which is treated as a (virtual) hadron whose structure is probed by the virtual photon. The pomeron is described by a structure function $F_2^{I\!P}(\beta, Q^2)$ which is independent of the process of emission. In this sense factorisation is predicted in the model:

$$F_2^{D(4)}(\beta, Q^2, x_{I\!P}, t) = f_{I\!P}(x_{I\!P}, t) \cdot F_2^{I\!P}(\beta, Q^2).$$

The flux factor $f(x_{I\!P}, t)$, describing the flux of pomerons in the proton, can be extracted from hadron-hadron scattering with an accuracy of approximately 30%, assuming universality of the pomeron flux. A comparison of different flux factors can be found in [29].

For this analysis we used the POMPYT Monte Carlo implementation [27] of the Ingelman-Schlein model. Two samples of events were generated, corresponding to a hard quarkonic structure function,

$$F_2^{I\!P}(\beta, Q^2) = \sum_{q_i} e_i^2 \beta f_q(\beta, Q^2) = \frac{5}{3} \cdot \beta(1 - \beta),$$

and to a soft quarkonic structure function,

$$F_2^{I\!P}(\beta, Q^2) = \sum_{q_i} e_i^2 \beta f_q(\beta, Q^2) = \frac{5}{3} \cdot (1 - \beta)^5.$$

The two samples are denoted by "Hard Pomeron" (HP) and "Soft Pomeron" (SP) respectively. The normalisation constant $5/3$ is based on the assumption that the momentum sum rule (MSR) is satisfied for two light quark flavours (u,d). If s quarks would have to be included the normalisation factor would be reduced from $5/3$ to $4/3$ [31]. The $Q^2$ dependence is expected to be weak and is neglected. The Ingelman-Schlein form of the flux is parametrised by a fit to UA4 data [27, 30]:

$$f_{I\!P}(x_{I\!P}, t) = \frac{1}{2} \frac{1}{2.3 \cdot x_{I\!P}} \cdot (6.38 \ e^{8t} + 0.424 \ e^{3t}).$$

In the Donnachie-Landshoff (DL) model diffraction in DIS is described through pomeron exchange between the virtual photon and the proton, with the pomeron coupling predominantly to quarks [32]. The authors calculate the cross section in the framework of Regge theory. The result can be interpreted in terms of a pomeron structure function with the resulting $\beta$ dependence similar to HP but with a normalisation which is calculated to be approximately a factor of 6.2 smaller. The authors also predict an additional soft contribution to the pomeron structure function which is expected to become important only for $\beta < 0.1$. The flux factor,

$$f_{I\!P}(x_{I\!P}, t) = \frac{9\beta_0^2}{4\pi^2} F_1(t)^2 x_{I\!P}^{1-2\alpha(t)},$$

is related to the elastic form factor of the proton, $F_1(t) = \frac{4M^2 - 2.8t}{4M^2 - t}(\frac{1}{1-t/0.7})^2$, and to the pomeron-quark coupling, $\beta_0 \simeq 1.8$ GeV$^{-1}$, extracted from hadron-hadron data. The $x_{I\!P}$ term represents the pomeron propagator with the pomeron trajectory, $\alpha(t) = 1.085 + 0.25 \cdot t$. Therefore the $x_{I\!P}$ dependence of $F_2^{D(4)}$ is controlled by the pomeron trajectory ($F_2^{D(4)} \propto x_{I\!P}^{1-2\alpha(t)}$). Integrated over $t$, the predicted effective $x_{I\!P}$-dependence at fixed $\beta$ is approximately $(1/x_{I\!P})^{1.09}$ in the measured range of $x_{I\!P}$.

In a recent publication [33] Goulianos proposed to use a modified flux factor, which is renormalised to unity for fixed centre-of-mass energy $W$. Also a modification of the $t$-dependence and the pomeron trajectory according to recent CDF data [34] is proposed:

$$f_{I\!P}(x_{I\!P}, t) = \frac{1}{N_0} \cdot 0.73 \cdot e^{4.6t} \cdot x_{I\!P}^{1-2\alpha(t)},$$

where $\alpha(t) = 1.115 + 0.26 \cdot t$ and $N_0$ is a normalisation factor which can be approximated by $(\frac{W^2}{400})^{0.23}$. Integrated over $t$, the effective $x_{I\!P}$-dependence of this flux factor is approximately $(1/x_{I\!P})^{0.93}$.

Capella et al. calculate the diffractive structure function in the framework of conventional Regge theory [24]. Using Regge factorisation, they relate the pomeron structure function to

6

the deuteron structure function using parameters which are determined from soft hadronic diffraction data with an appropriate change for the disappearance of screening corrections with increasing $Q^2$. For $Q^2 = 10$ GeV$^2$ they obtain:

$$F_2^{I\!P}(\beta, Q^2) = a \cdot \beta^{0.6} \cdot (1 - \beta)^{0.6} + 0.015 \cdot \beta^{-0.22} \cdot (1 - \beta)^{4.6} \,,$$

where $a$ is estimated to be in the range 0.04 to 0.06. We chose $a = 0.06$ for comparison with the data.

In the model of Nikolaev and Zakharov diffractive dissociation is described as a fluctuation of the photon into a $q\bar{q}$ or $q\bar{q}g$ Fock state [25, 26]. The interaction with the proton proceeds via the exchange of a BFKL [35] type pomeron, starting in lowest-order from the exchange of a Low-Nussinov [4] pomeron which corresponds to two gluons in a colour-singlet state. The result for the cross section can be approximated by a two-component structure function of the pomeron, each component having its own flux factor. This corresponds to factorisation breaking which is caused by BFKL evolution effects. The result for the "hard" component reflects the case where the photon fluctuates into a $q\bar{q}$ pair and leads to a $\beta$ dependence similar to that of the HP and the DL models with a normalisation closer to the latter (but with very different predictions for the contribution of heavy flavours). The "soft" contribution, which reflects the case where the photon fluctuates into $q\bar{q}g$, is assumed to be proportional to $(1 - \beta)^2$ and the normalisation is fixed by the triple pomeron coupling. The relative size of these contributions and the overall normalisation are predicted with an uncertainty of about 30%. $Q^2$ evolution effects have been calculated for this model, and have been found to be rather weak for $\beta > 0.1$. We used a Monte Carlo implementation of this model [28] which is based on the cross section given in [25] and is interfaced to the Lund fragmentation scheme. We refer to this model as NZ. In this implementation the mass spectrum contains both components but the $q\bar{q}g$ states are fragmented into hadrons as if they were a $q\bar{q}$ system with the same $M_X$.

Both Monte Carlo generators have limitations in the generation of small masses $M_X$ ($M_X < 1.7$ GeV for NZ and $M_{X'} < 5$ GeV for POMPYT, where $M_{X'}$ includes the final state electron). We exclude these regions for the measurement of the diffractive structure function by an upper cut on $\beta$. To study acceptance and migration effects for these small masses we have generated an additional sample of exclusively produced $\rho^0$'s [36].

The cuts given below to select diffractive events limit the acceptance for double-dissociative events, where the proton also dissociates. The PYTHIA Monte Carlo [37] has been used to study the detector response for the nucleon system $M_N$ in double dissociation $\gamma p$ events. The nucleon system mass spectrum and the fraction of double-dissociative to single-dissociative events was taken from hadron data.

Non-diffractive DIS processes were generated using the HERACLES 4.4 program [38] which incorporates first order electroweak corrections. The Monte Carlo generator LEPTO 6.1 [39], interfaced to HERACLES via the program DJANGO 6.0 [40], was used to simulate QCD cascades and fragmentation. The parton cascade was modelled with the colour-dipole model including the boson-gluon fusion process by the ARIADNE 4.03 [41] (CDMBGF) program. The fragmentation into hadrons was performed with the Lund string hadronisation model [42] as implemented in JETSET 7.2 [43]. For the proton parton densities the MRSD$'_{-}$ set [44] was chosen, which adequately represents our structure function results [18]. In previous studies [45] it was shown that this model gives a good description of the energy flow between the current jet and the remnant jet.

Combined sets of the Monte Carlo generators, described above, were used to simulate the expected final states in our DIS sample: the first one to describe non-diffractive DIS processes and the second one to model diffractive events.

QED radiative processes were not simulated for diffractive events; however, with the selection cuts of section 6, radiative corrections to the DIS cross sections are below 10% [18] and are expected to be of the same order for diffractive processes. All Monte Carlo events were passed through the standard ZEUS detector and trigger simulations and the event reconstruction package [10]. According to Monte Carlo studies, the efficiency of the trigger and of the final selection cuts is the same for diffractive and non-diffractive DIS events. The overall trigger acceptance is above 95%, independent of $x$ and $Q^2$ in the range of interest for this analysis.

# 6    Event selection

The selection of DIS events was similar to that described in our earlier publications [1, 18]. The following offline cuts were applied:

- $E'_e \geq 5$ GeV, to ensure good electron identification;

- $Q^2_{DA} \geq 8$ GeV$^2$;

- $y_{JB} \geq 0.04$, to give sufficient accuracy for DA reconstruction;

- $\delta \geq 35$ GeV (with respect to the measured interaction point), to reduce radiative corrections and photoproduction background;

- $y_e \leq 0.95$, to reduce photoproduction background;

- the impact point of the electron on the face of the RCAL was required to lie outside a square of side 32 cm centred on the beam axis (box cut), to ensure that the electron shower was fully contained within the calorimater and its position could be reconstructed with sufficient accuracy;

- a vertex, as reconstructed from VXD+CTD tracks, was required with $|Z_{vtx}| \leq 40$ cm.

In addition algorithms were used to reject cosmic-ray induced events and QED Compton events.

A total of 31k events was selected in this way corresponding to an integrated luminosity of 0.54 pb$^{-1}$. Using the number of events produced by unpaired electron and proton bunches, the contamination from beam-gas background and from cosmic-ray muons were estimated to be less than 1% each. The background in the total DIS sample due to photoproduction was estimated to be $(2.5 \pm 1)\%$ from a fit to the shape of the $\delta$ distribution before the above cut on $\delta$ was applied [18].

# 7    Properties of diffractive events

In the following section, the observed data distributions are compared to distributions from various Monte Carlo models. We discuss the criteria used to select the diffractive events, the methods used to determine their relative contribution and the observed inclusive distributions of the diffractive sample.

## 7.1    Selection criterion

A large fraction of diffractive processes at HERA exhibit a rapidity gap in the main detector between the scattered proton system and the hadronic activity generated by the dissociation of the photon, while large rapidity gaps are suppressed in non-diffractive DIS events. Therefore the presence of a rapidity gap has been used as a selection criterion [1, 2]. An improved criterion to separate diffractive from non-diffractive events is presented here, which uses the direction of the total hadronic energy flow of the event, determined from all the detected particles in the final state.

We define the maximum pseudorapidity of an event, $\eta_{\max}$, as the maximum value of the pseudorapidity of all calorimeter condensates with energy greater than 400 MeV or tracks with momentum of at least 400 MeV/c. A condensate is a contiguous energy deposit above a minimum energy threshold. We studied the effect of varying the minimum energy $E_{\min} = 400$ MeV and found that above $E_{\min} = 200$ MeV the $\eta_{\max}$ distribution does not change significantly. We chose $E_{\min} = 400$ MeV as a conservative compromise between accepting diffractive events and rejecting noise.

For values of $\eta_{\max}$ up to 1–1.5 the non-diffractive DIS background is a negligible background to the diffractive sample, which increases for values of $\eta_{\max}$ above 1.5–2. In previous ZEUS publications [1, 2] diffractive events were selected by $\eta_{\max} < 1.5$. This cut selects a rather pure sample of diffractive events, useful to establish a signal but it limits acceptance for events with large $M_X$.

The $\eta_{\max}$-cut is dependent on the most forward condensate but does not use the information from the full energy flow. Larger acceptance can be achieved by including more information from the hadronic energy flow. Since in diffractive scattering the proton remains intact or, in the case of double-dissociative events, dissociates independently from the photon, the hadronic activity in the detector in general will not follow the proton direction. The hadronic angle $\theta_H$ defined in eq. (1) represents the average direction of the hadronic activity. Non-diffractive DIS events have mostly $\cos\theta_H$ near 1 because of the colour flow between the struck quark and the outgoing proton system, while a substantial fraction of diffractive events is found at $\cos\theta_H$ less than 1. Figures 2a, b show scatter plots of $\eta_{\max}$ versus $\theta_H$ for the diffractive and non-diffractive DIS Monte Carlo samples. A cut $\cos\theta_H < 0.75$ combined with $\eta_{\max} < 2.5$ allows a larger acceptance of diffractive events than the $\eta_{\max} < 1.5$ cut, at the price of a slightly higher background which has to be subtracted. We call this combined cut, used to select the diffractive sample, the $\eta_{\max}$-$\theta_H$ cut.

Note that the term "diffractive" is used to indicate single diffractive dissociation of the photon together with that fraction of events where both the photon and the proton dissociate and the proton system is not detected. From proton-proton measurements of the ratio of double- to single-dissociative events, we estimate this ratio to be approximately 0.76 in the measured $W$ range. As shown in Fig. 3, we find that excited proton states with mass $M_N \lesssim 4$ GeV would pass the diffractive selection cuts. Beyond this range the energy deposition in the forward calorimeter is typically above 400 MeV. The overall acceptance for double-dissociative events is 23%. We therefore have an estimated double-dissociative contribution of $\simeq (15\pm10)\%$ which is expected to be independent of $\beta$ and $Q^2$ and not vary significantly with $x_{I\!P}$. This result assumes factorisation in Regge theory, i.e. that the nucleon mass spectrum and the ratio of double- to single-dissociative events is similar to that measured in proton-proton collisions at similar energies.

## 7.2 Estimation of the diffractive component

In this section, only the shapes of the distributions and not the absolute normalisations of the diffractive models are considered. The $\eta_{\max}$ and $\theta_H$ distributions are used to determine the fraction of diffractive events passing the DIS selection criteria. A linear combination of diffractive DIS (NZ or POMPYT) and non-diffractive DIS Monte Carlo events are fitted to the data.

The $\eta_{\max}$ and $\theta_H$ distributions were first fitted separately to check consistency between the results and then together to obtain a global result. Figure 4 shows the fits to these distributions. The part of each distribution that corresponds to the forward region of the detector (high values of $\eta_{\max}$ and low values of $\theta_H$) was put into one single bin to reduce problems associated with a detailed description of the hadronisation of the proton remnant. For each distribution a variety of different binnings was tried and the results were found to be stable.

| Model | $\eta_{\max}$ | | $\theta_H$ | | $\eta_{\max}+\theta_H$ | |
|---|---|---|---|---|---|---|
| | % of diffr. | $\chi^2_{dof}$ | % of diffr. | $\chi^2_{dof}$ | % of diffr. | $\chi^2_{dof}$ |
| NZ | $14.2 \pm 2.5$ | 4.7 | $15.3 \pm 2.5$ | 4.0 | $14.8 \pm 3.0$ | 4.3 |
| SP | $35.9 \pm 7.0$ | 10.5 | $15.4 \pm 2.6$ | 5.0 | $33.0 \pm 6.0$ | 24 |
| HP | $10.3 \pm 2.0$ | 2.2 | $10.8 \pm 2.0$ | 4.1 | $10.5 \pm 2.7$ | 3.0 |
| HP+SP | $15.6 \pm 1.3$ | 3.7 | $13.4 \pm 1.3$ | 5.4 | $14.6 \pm 1.4$ | 4.6 |

Table 1: Fraction of diffractive events and $\chi^2$ per degree of freedom ($\chi^2_{dof}$) values obtained from fits using NZ, SP, HP or HP+SP.

The results are summarised in Table 1, where the default parameters have been used for the models. Since neither NZ nor POMPYT describes diffractive vector meson production a simulation of exclusive $\rho^o$ production was added in order to incorporate the effect of low-mass states. This contribution was estimated to be typically $\sim 7\%$ of the diffractive sample from a fit to the observed $M_X$ spectrum in different $Q^2$ intervals. For each model, a reduction of $\chi^2_{dof}$ by 1–2 was found when $\rho^o$ production was included, with consistent results obtained for the fraction of diffractive events.

The SP model was also extensively tested. In fits to the $\eta_{\max}$ and $\theta_H$ distributions, SP does not reproduce the shapes correctly. Its very soft $\beta$ distribution tends to populate large $\eta_{\max}$ bins and, consequently, the fits do not describe the data. The inconsistency of the results obtained by the fits to the $\eta_{\max}$ and the $\theta_H$ distributions shown in Table 1 indicate that a pure soft $\beta$ distribution cannot describe the data. For these reasons the SP model alone is not considered any further. Results obtained with the combined HP+SP model, discussed in the following section, are also given in Table 1. The fractions obtained with the HP+SP model are similar to those determined using the NZ model.

It is possible to explain the different predictions from NZ and HP models in terms of the $\beta$ distribution used in these models: they both contain the hard component responsible for low $\eta_{\max}$ (high $\theta_H$) events but the NZ model also contains a soft contribution which is predicted to be $\sim 40\%$ of the diffractive cross section. Most of the events originating from this soft component are hidden under the large background from normal DIS events and so are not accessible to the present study.

## 7.3 Inclusive distributions

In the following, the shapes of the observed distributions in $W$, $Q^2$, $x$, $M_X$, $x_{I\!\!P}$ and $\beta$ are considered. The relative normalisation of the models is obtained from the above fits. It should be noted that the normalisation of the non-diffractive component, which is relevant for the background subtraction, is independent of the diffractive model used to fit the data to within 5%.

In order to confine the analysis to regions of acceptance above $\simeq 80\%$, the following $(M_X, y)$ intervals were considered:

$$
\begin{aligned}
M_X &< 10 \text{ GeV} \quad \text{for} \quad 0.08 < y < 0.2 \\
M_X &< 16 \text{ GeV} \quad \text{for} \quad 0.2 < y < 0.3 \\
M_X &< 20 \text{ GeV} \quad \text{for} \quad 0.3 < y < 0.8
\end{aligned}
$$

According to Monte Carlo studies, the $\eta_{\max}$-$\theta_H$ cut reduces the non-diffractive DIS component by $\simeq 60\%$ and the diffractive component by $\simeq 20\%$, giving a contamination from non-diffractive DIS of less than 15% in these $(M_X, y)$ intervals. This background is subtracted from the data before comparison with the diffractive Monte Carlo predictions.

Figure 5 shows the $x$, $Q^2$, W, $x_{I\!\!P}$, $M_X$ and $\beta$ distributions after applying the $\eta_{\max}$-$\theta_H$ cut, requiring the data to be in the accepted ranges of $(M_X, y)$ and subtracting the DIS background indicated in the figure. The errors on the data points are calculated by summing in quadrature the statistical error (which is the dominant error) and 50% of the total subtracted DIS background (which is taken as a conservative estimate of the uncertainty due to the DIS background). In addition, the predictions from the two diffractive models (NZ and HP) are shown.

In general, both models describe the data. Differences are observed in the $M_X$ and $\beta$ distributions, where the HP model underestimates the observed number of events at low $\beta$ values and does not reproduce the observed $M_X$ distribution at large $M_X$. The NZ model, incorporating a soft component, describes the observed $\beta$ and $M_X$ distributions.

A pure "hard" $\beta$ distribution cannot account for the data, therefore, the observed $\beta$ spectrum was fitted as a sum of a "hard + soft" contribution from the POMPYT Monte Carlo. This resulted in a contribution of $\simeq 60\%$ and $\simeq 40\%$ from HP and SP, respectively. This HP+SP model is also shown in Fig. 5. Comparison with the data indicates that such a model also describes the observed $\beta$ behaviour.

To investigate the $\beta$ distribution in more detail, each $(M_X, y)$ interval was divided into two $Q^2$ bins:

$$Q^2 = 8 - 20, \ 20 - 160 \text{ GeV}^2$$

The results, together with the predictions from the diffractive models are shown in Fig. 6. In general, the Monte Carlo models reproduce the shape of the data reasonably well. However, in the high-$y$ and low-$Q^2$ intervals where the mass extends to larger values (Fig. 6a and c), the soft contribution is important. The NZ model describes the data best in this region. The HP+SP model reasonably describes the data and gives an improved description compared to the HP model in each $(M_X, y)$ interval.

Using the NZ model, the combined fit to the $\eta_{\max}$ and $\theta_H$ distributions was performed in bins of $W$ and $x$ respectively, separately for the two $Q^2$ intervals indicated above, to extract the fraction of diffractive events as a function of these variables. Figure 7 shows the diffractive fraction as a function of $W$ and $x$ for different values of $Q^2$. The results extracted using the HP+SP model agree within statistical errors. The results extracted using the HP model give a normalisation which is $\simeq 30\%$ lower, but with the same dependence on $x$, $W$ and $Q^2$. The fits are mainly sensitive to the hard component: a large uncertainty on the diffractive contribution to the DIS sample comes from the soft part in the pomeron structure function, which is suppressed by the applied cuts, especially at small values of $W$. In all cases, no strong dependence of this ratio is observed as a function of $x$, $W$ or $Q^2$.

# 8 Measurement of the diffractive structure function

As described in section 4, the differential cross section can be expressed in terms of the diffractive structure function $F_2^{D(3)}$ as a function of $\beta$, $x_{I\!P}$ and $Q^2$. In this section, we discuss the resolution of the measured quantities and describe the kinematic region chosen. We finally discuss the systematic errors and present the results of the measurement of $F_2^{D(3)}$.

## 8.1 Extraction of $F_2^{D(3)}$

According to Monte Carlo studies (see section 5), the resolution of $Q^2$ is 25%, independent of $Q^2$. The resolution of $x$ varies smoothly with $x$ from 20% at $x = 10^{-2}$ to 50% at $10^{-3}$, almost independent of $Q^2$. The resolution of $M_X$, reconstructed with the method described in section 3, is approximately 27%, independent of $M_X$. The $M_X$ reconstruction is affected by energy loss in inactive material in front of the calorimeter and the position determination of hadrons. In order to reduce migrations at small masses, the cell energy thresholds for isolated cells were increased. Monte Carlo studies show that, except for very small masses ($< 3$ GeV) where calorimeter noise becomes important, $M_X$ is systematically shifted by 10% to smaller values, independent of $y$ and $Q^2$. In order to compensate for this shift, a correction factor of 1.10 was applied to the measured $M_X$ values for the determination of the diffractive structure function. The resolution of $x_{I\!P}$ is approximately 25%. The resolution of $\beta$ varies smoothly with $\beta$ from 40% at $\beta = 0.1$ to 20% at $\beta = 0.8$.

Below $Q^2$ of 8 GeV$^2$, the event acceptance drops below 50% due to the box cut requirement. The statistics of the 1993 data allow four ranges in $Q^2$ to be selected above this lower limit. The migration of events is large at small values of $x$: we therefore chose bins where the central $x$-value is above $4 \cdot 10^{-4}$. The acceptance of the diffractive component increases as a function of $y$: we therefore select only bins with $y > 0.08$. The overall acceptance due to the DIS and diffractive cuts in the selected bins given in Table 2 is always greater than 50% and typically $\simeq 80\%$. The $M_X$ resolution determines the chosen bin size in the variables $\beta$ and $x_{I\!P}$. The purity, defined as the fraction of simulated events generated in a bin and measured in the same bin, is always greater than 25% and typically $\simeq 40\%$ in each of the selected bins.

In order to control the influence of photoproduction background, radiative corrections and $F_L$ contributions, we restrict our analysis to $y < 0.5$. As a consequence the minimum scattered electron energy requirement is raised to 10 GeV. We checked that our sensitivity to $F_L$ is smaller

than the quoted errors in all bins. Furthermore, the region $\beta < 0.8$ is selected to exclude the region of low masses where vector meson production is dominant.

The level of photoproduction background is estimated in bins of $x_{I\!P}$ and $Q^2$ by fits to the $\delta$ distributions (see [18] for details). Since it is typically $\simeq 1\%$ and always below $4\%$ we do not correct for this background.

We select bins with $x_{I\!P} < 0.01$ and $\beta > 0.1$ where the non-diffractive component can be safely estimated. In each of the bins the number of events is then evaluated by subtraction of the estimated number of DIS background events, based on the ARIADNE Monte Carlo program with the normalisation described in section 6. The contribution of the DIS background is given in Table 2.

To unfold the effects of acceptance and event migration we used the NZ Monte Carlo event sample, which gives a good description of our data. For this initial study we used a one-step matrix unfolding procedure and applied a bin-centring correction for the quoted $F_2^{D(3)}$ values.

## 8.2 Systematic errors

Several systematic checks were performed to estimate the uncertainties due to the selection cuts, background estimate and the unfolding. Systematic errors due to the DIS event selection were evaluated in the following way (see [18] for a detailed discussion):

- different algorithms were used to identify the scattered electron which differ in purity and efficiency. The changes to $F_2^{D(3)}$ were below 10%;

- the cut on $E'_e$ was decreased from 10 to 5 GeV to study the effect of a possible mismatch of the shower profiles of data and Monte Carlo at small energies. The change of $F_2^{D(3)}$ was less than 5% in each bin;

- the box-cut was changed by 2 cm from the nominal values, to study the effects of electron position reconstruction at small angles. This resulted in changes which were always less than 15%;

- the $\delta$-cut was raised from 35 GeV to 40 GeV, to study the effect of radiative corrections, which were not included in the simulations. This resulted in a general shift of $\simeq 10\%$ towards smaller $F_2^{D(3)}$ values;

- the $y_{JB}$-cut was changed from 0.04 to 0.02 and to 0.06. This affected the region of large $x_{I\!P}$ where $F_2^{D(3)}$ changes by about 10%.

Systematic errors due to the diffractive event selection were evaluated in the following way:

- the effect of a possible mismatch between the hadronic energy scale in the Monte Carlo and the data was investigated by shifting the hadron energy scale by 7% in the Monte Carlo simulation. The use of the $DA$ variables resulted in changes on $F_2^{D(3)}$ which were always smaller than 2%;

13

- the fraction of low-mass events was reduced by 50%. Due to migrations from $\beta > 0.8$, this change influences the small $Q^2$, high $\beta$ bin, where the values were shifted upwards by $\simeq 10\%$;

- the HP model was used instead of the NZ simulation for unfolding the data. Some effect was seen in the small $\beta$-region, where the pomeron structure functions differ. The changes to $F_2^{D(3)}$ were typically $\simeq 10\%$;

- as a systematic check for the estimate of the DIS background the $\eta_{\mathrm{max}}$-cut was reduced from 2.5 to 2.0 resulting in changes of up to 20% in the highest $x_{I\!P}$ bins. The $\eta_{\mathrm{max}}$-cut was also increased from 2.5 to 3.0 resulting in changes of up to 10%;

- similarly, the $\theta_H$ cut was removed, yielding changes below 5%;

- the cells with $\eta > 2.5$ were removed to check the dependence on the double-dissociative contribution, resulting in changes which were up to 5%.

Overall most of these checks yielded results which agree with the standard method within statistical errors. The differences of the DIS and diffractive systematic checks compared to the standard method were combined in quadrature to yield the quoted systematic errors.

## 8.3   Results

Table 2 summarises the results for $F_2^{D(3)}$, for the 0.54 pb$^{-1}$ ($\pm 3.5\%$) integrated luminosity. The statistical errors include statistical uncertainties from the Monte Carlo models used for the unfolding.

The $F_2^{D(3)}$ results are displayed in Fig. 8. The data are observed to fall rapidly as a function of increasing $x_{I\!P}$. In the measured bins the dependence of $F_2^{D(3)}$ on $Q^2$ at fixed $\beta$ values is weak. We have investigated whether the $x_{I\!P}$-dependence of $F_2^{D(3)}$ is the same in each $\beta, Q^2$ interval, as expected if factorisation holds. For this purpose we performed fits of the form:

$$b_i \cdot (1/x_{I\!P})^a$$

where the normalisation constants $b_i$ were allowed to differ, while the exponent was the same for each $\beta, Q^2$ interval. The result of the fit was:

$$a = 1.30 \pm 0.08 \ (stat) \ {}^{+}_{-} \ {}^{0.08}_{0.14} \ (sys).$$

The systematic errors are calculated by re-fitting the $F_2^{D(3)}$ values according to the variations listed in section 8.2 and combining the positive or negative deviations from the central value of $a$ in quadrature. The overall statistical $\chi^2$ values of these fits are in the range 8.2–14.0 for 23 degrees of freedom depending on the systematic check. The $\chi^2$ values for each of the $\beta, Q^2$ intervals are in the range 0.1–1.1 per degree of freedom. Within the present accuracy, the data are therefore consistent with the assumption of factorisation in the measured kinematic range. The value of $a$ is consistent with recent results from the H1 Collaboration of $a = 1.19 \pm 0.06 \pm 0.07$ [9].

The observed dependence on $x_{I\!P}$ is steeper but still compatible with a Donnachie-Landshoff type of flux factor which yields $a \simeq 1.09$ and which is based on a phenomenological description of "soft hadronic" diffractive interactions. The modified flux of Goulianos yields a $(1/x_{I\!P})^a$ dependence with $a \simeq 0.93$, a value which is disfavoured by the data.

In order to illustrate the $\beta$ and $Q^2$ dependence of $F_2^{D(3)}(\beta, Q^2, x_{I\!P})$, we integrated $F_2^{D(3)}$ over the measured range of $x_{I\!P}$, $6.3 \cdot 10^{-4} < x_{I\!P} < 10^{-2}$, using the fitted $x_{I\!P}$ dependence. The resulting values of $\tilde{F}_2^D(\beta, Q^2)$ are shown in Fig. 9 as a function of $\beta$ and $Q^2$. It should be noted that these results assume that a universal $x_{I\!P}$ dependence holds in *all* regions of $\beta$ and $Q^2$. In particular, there is a contribution due to regions of $x_{I\!P}$ which are not measured and where the hypothesis of a universal $x_{I\!P}$ dependence has not been tested experimentally.

The $\tilde{F}_2^D(\beta, Q^2)$ values as a function of $\beta$ for fixed $Q^2$ are consistent with a flat $\beta$ dependence as expected from the aligned jet model [46] and the model of Buchmüller [47]. As a function of $Q^2$ for fixed $\beta$, the $\tilde{F}_2^D(\beta, Q^2)$ values are approximately independent of $Q^2$ for all $\beta$ values, which is consistent with a picture where the underlying interaction is the scattering of a virtual photon with point-like quarks within the pomeron.

As a next step we determined a compact parametrisation for the $F_2^{D(3)}$ results, which is also shown in Fig. 8 and Fig. 9, where the following form was adopted:

$$F_2^{D(3)} = (1/x_{I\!P})^a \cdot b \cdot \left(\beta(1-\beta) + \frac{c}{2} \cdot (1-\beta)^2\right),$$

with $a = 1.30$. This parametrisation assumes factorisation and no $Q^2$-dependence. The soft contribution to the structure function was considered by the inclusion of the $(1-\beta)^2$ term. The multiplicative factor of $\frac{c}{2}$ was chosen such that the integral over $\beta$ of the soft contribution is equal to that of the hard contribution when $c = 1$. The power of 2 was adopted from the NZ model; this assumption cannot be tested with the current measurement. The results of the fit were:

$$b = 0.018 \pm 0.001 \ (stat) \pm 0.005 \ (sys),$$

$$c = 0.57 \pm 0.12 \ (stat) \pm 0.22 \ (sys),$$

with a statistical $\chi^2$ in the range 15–23 for 33 degrees of freedom depending on the systematic check. A fit without the $(1-\beta)^2$ soft contribution resulted in $\chi^2$ values in the range 56–81 for 34 degrees of freedom. This increased $\chi^2$ value indicates that a soft component is required in the pomeron structure function.

We now consider the cross section predictions of the models discussed in section 5. The $F_2^{D(3)}$ results are displayed in Fig. 10 where the data are compared with the predictions of several models of single-diffractive dissociation for which the momentum sum rule for quarks is not satisfied. The estimated 15% fraction of double-dissociative events has been subtracted in order to compare with these models.

At high $\beta$-values the predictions of Nikolaev-Zakharov, Donnachie-Landshoff and Capella et al. underestimate the observed values slightly, but are generally in reasonable agreement. At smaller $\beta$-values, the Donnachie-Landshoff parametrisation, which includes only a hard component of the pomeron structure function, underestimates the observed $F_2^{D(3)}$. The Capella et al. and Nikolaev-Zakharov predictions, which also include a soft component, are able to give a fair description at smaller $\beta$-values. The factorisation-breaking effects in the model

of Nikolaev-Zakharov, which occur at small $\beta$ values, are too small to be observable in this analysis.

In Fig. 11 the data are compared with a model for which the momentum sum rule for the pomeron structure function is assumed for the light quark flavours (u,d) and the $\beta$ dependence is taken from the parametrisation, discussed above. Adopting the Donnachie-Landshoff flux factor, the observed $F_2^{D(3)}$ is about a factor three to four below the expectation if the momentum sum rule is assumed to be fulfilled only by quarks. An uncertainty arises from the choice of the pomeron flux factor: if the Ingelman-Schlein form for the flux factor is adopted then the prediction is reduced by approximately 30%. Even if the Goulianos prescription for the flux is adopted, the observed $F_2^{D(3)}$ results are always below the predictions. These comparisons indicate that in an Ingelman-Schlein type model the quarks alone inside the pomeron do not satisfy the momentum sum rule.

# 9    Conclusions

The properties of diffractive DIS events with $Q^2 > 8$ GeV$^2$, selected by a large rapidity gap requirement, have been investigated. Different Monte Carlo models, such as the POMPYT model, with a soft plus a hard pomeron structure function, or the Nikolaev-Zakharov model describe the shape of the observed kinematic distributions. Using these models, reliable acceptance corrections for the measured data can be obtained and corrected cross sections can be determined. The relative contribution of diffractive events to the total DIS cross section is found to have no strong dependence on $x$, $W$ or $Q^2$.

The diffractive proton structure function $F_2^{D(3)}$ is presented, integrated over $t$, the square of the momentum transfer at the proton vertex, as a function of $x_{I\!\!P}$, the momentum fraction lost by the proton, of $\beta$, the momentum fraction of the struck quark with respect to $x_{I\!\!P}$, and of $Q^2$. The structure function is measured in the kinematic range of $0.08 < y < 0.5$, $8 < Q^2 < 100$ GeV$^2$, $6.3 \cdot 10^{-4} < x_{I\!\!P} < 10^{-2}$ and $0.1 < \beta < 0.8$. Within the experimental errors, the measurement is consistent with models where diffraction is described by the exchange of a particle-like pomeron where the structure function factorises into a pomeron flux factor, which depends on $x_{I\!\!P}$ and a pomeron structure function, which is independent of $x_{I\!\!P}$. The diffractive structure function is also well-described by the Nikolaev-Zakharov model, which does not require the concept of a particle-like pomeron, in terms of overall normalisation and dependence on the kinematic variables, $x_{I\!\!P}$, $\beta$ and $Q^2$. The $x_{I\!\!P}$ dependence is consistent with the form $(1/x_{I\!\!P})^a$ where $a = 1.30 \pm 0.08\ (stat)\ {}^{+\ 0.08}_{-\ 0.14}\ (sys)$ in all bins of $\beta$ and $Q^2$. The value of $a$ is slightly higher but compatible with that obtained from hadron-hadron interactions and in agreement with recent results from the H1 collaboration. In the measured $Q^2$ range, the pomeron structure function is approximately independent of $Q^2$ at fixed $\beta$ consistent with an underlying interaction where the virtual photon scatters off point-like quarks within the pomeron. The $\beta$-dependence of the pomeron structure function requires both a hard and a soft component. In an Ingelman-Schlein type model, where commonly used pomeron flux factor normalisations are assumed, it is found that the quarks within the pomeron do not saturate the momentum sum rule.

# Acknowledgements

# References

[1] ZEUS Collab., M. Derrick et al., Phys. Lett. B315 (1993) 481.

[2] ZEUS Collab., M. Derrick et al., Phys. Lett. B332 (1994) 228.

[3] K. Goulianos, Nucl. Phys. B (Proc. Suppl.) 12 (1990) 110.

[4] F. E. Low, Phys. Rev. D12 (1975) 163;
    S. Nussinov, Phys. Rev. Lett. 34 (1975) 1286 and Phys. Rev. D14 (1976) 246.

[5] G. Ingelman and P. Schlein, Phys. Lett. 152B (1985) 256.

[6] UA8 Collab., R.Bonino et al., Phys. Lett. B211 (1988) 239;
    UA8 Collab., A.Brandt et al., Phys. Lett. B297 (1992) 417.

[7] ZEUS Collab., M. Derrick et al., Phys. Lett. B346 (1995) 399.

[8] H1 Collab., T. Ahmed et al., Phys. Lett. B435 (1995) 3.

[9] H1 Collab., T. Ahmed et al., DESY 95-036.

[10] The ZEUS Detector, Status Report 1993, DESY 1993.

[11] ZEUS Collab., M. Derrick et al., Phys. Lett. B293 (1992) 465.

[12] C. Alvisi et al., Nucl. Instrum. Methods A305 (1991) 30.

[13] C.B. Brooks et al., Nucl. Instrum. Methods A283 (1989) 477;
     N. Harnew et al., ibid. A279 (1989) 290;
     B. Foster et al., ibid. A338 (1994) 254.

[14] A. Andresen et al., Nucl. Instrum. Methods A309 (1991) 101.

[15] A. Bernstein et al., Nucl. Instrum. Methods A336 (1993) 23.

[16] A. Caldwell et al., Nucl. Instrum. Methods A321 (1992) 356.

[17] J. Andruszków et al., DESY 92-066.

[18] ZEUS Collab., M. Derrick et al., Z. Phys. C65 (1995) 379.

[19] S. Bentvelsen, J. Engelen and P. Kooijman, Proceedings of the Workshop on Physics at HERA, DESY Vol. 1 (1992) 23.

[20] F. Jacquet and A. Blondel, Proceedings of the Study for an $ep$ facility for Europe, DESY 79/48 (1979) 391.

[21] W. Buchmüller and A. Hebecker, DESY 95-077.

[22] G. Ingelman and K. Jansen-Prytz, Proceedings of the Workshop on Physics at HERA, DESY Vol. 1 (1992) 233;
G. Ingelman and K. Jansen-Prytz, Z. Phys. C58 (1993) 285.

[23] A. Donnachie and P.V. Landshoff, Nucl. Phys. B244 (1984) 322.

[24] A. Capella et al., Phys. Lett. B343 (1995) 403.

[25] N.N. Nikolaev and B.G. Zakharov, Z. Phys. C53 (1992) 331.

[26] M. Genovese, N.N. Nikolaev and B.G. Zakharov, KFA-IKP(Th)-1994-37 and CERN–TH.13/95.

[27] POMPYT 1.0: P. Bruni and G. Ingelman (unpublished);
DESY 93-187; Proceedings of the Europhysics Conference on HEP, Marseille 1993, 595.

[28] A. Solano, Ph.D. Thesis, University of Torino 1993 (unpublished);
A. Solano, Proceedings of the International Conference on Elastic and Diffractive Scattering, Nucl. Phys. B (Proc. Suppl.) 25 (1992) 274;
P. Bruni et al., Proceedings of the Workshop on Physics at HERA, DESY Vol. 1 (1991) 363.

[29] K. Prytz, Z. Phys. C64 (1994) 79.

[30] UA4 Collab., M. Bozzo et al., Phys. Lett. 136B (1984) 217.

[31] T. Gehrmann and W.J. Stirling, Durham preprint DTP/95/26.

[32] A. Donnachie and P.V. Landshoff, Phys. Lett. B191 (1987) 309;
A. Donnachie and P.V. Landshoff, Nucl. Phys. B303 (1988) 634.

[33] K. Goulianos, Rockefeller University preprint RU 95/E-06.

[34] CDF Collab., F. Abe et al., Phys. Rev. D50 (1994) 5518.

[35] L.N. Lipatov, Sov. J. Nucl. Phys. 23 (1976) 338;
Y.Y. Balitsky and L. N. Lipatov, Sov. J. Nucl. Phys. 28 (1978) 822;
E.A. Kuraev, L. N. Lipatov and V. S. Fadin, Sov. Phys. JETP 45 (1977) 199.

[36] ZEUS Collab., M. Derrick et al., in preparation.

[37] PYTHIA 5.6: H.-U. Bengtsson and T. Sjöstrand, Comp. Phys. Comm. 46 (1987) 43.

[38] A. Kwiatkowski, H. Spiesberger and H.-J. Möhring, Proceedings of the Workshop on Physics at HERA, DESY Vol. 3 (1992) 1294.

[39] G. Ingelman, Proceedings of the Workshop on Physics at HERA, DESY Vol. 3 (1992) 1366.

[40] K. Charchuła, G. Schuler and H. Spiesberger, Comp. Phys. Comm. 81 (1994) 381.

[41] L. Lönnblad, Comp. Phys. Comm. 71 (1992) 15.

[42] B. Andersson et al., Phys. Rep. 97 (1983) 31.

[43] T. Sjöstrand, Comp. Phys. Comm. 39 (1986) 347;
T. Sjöstrand and M. Bengtsson, Comp. Phys. Comm. 43 (1987) 367.

[44] A.D. Martin, W.J. Stirling and R.G. Roberts, Phys. Lett. B306 (1993) 145.

[45] ZEUS Collab., M. Derrick et al., Phys. Lett. B338 (1994) 483.

[46] J.D. Bjorken and J. Kogut, Phys. Rev. D8 (1973) 1341.

[47] W. Buchmüller, Phys. Lett. B335 (1994) 479;
W. Buchmüller, DESY 95-065.

| $Q^2$ (GeV$^2$) | $\beta$ | $x_{I\!P}$ | #events | #non-diff. background | $F_2^{D(3)} \pm$stat. $\pm$ sys. |
|---|---|---|---|---|---|
| 10 | 0.175 | 0.0032 | 54 | 7.1 | $9.7 \pm 1.6 \pm 2.8$ |
| 10 | 0.175 | 0.0050 | 32 | 5.2 | $5.0 \pm 1.1 \pm 2.3$ |
| 10 | 0.375 | 0.0013 | 62 | 0.9 | $37.7 \pm 5.2 \pm 6.5$ |
| 10 | 0.375 | 0.0020 | 43 | 2.8 | $22.0 \pm 3.7 \pm 3.7$ |
| 10 | 0.375 | 0.0032 | 15 | 2.8 | $9.2 \pm 3.0 \pm 4.5$ |
| 10 | 0.65 | 0.00079 | 56 | 0.9 | $47.7 \pm 8.7 \pm 29.9$ |
| 10 | 0.65 | 0.0013 | 20 | 0.9 | $29.1 \pm 7.0 \pm 8.5$ |
| 10 | 0.65 | 0.0020 | 23 | 0 | $10.9 \pm 2.3 \pm 6.9$ |
| 16 | 0.175 | 0.0032 | 48 | 5.2 | $9.5 \pm 1.6 \pm 2.1$ |
| 16 | 0.175 | 0.0050 | 50 | 4.7 | $6.5 \pm 1.1 \pm 1.8$ |
| 16 | 0.175 | 0.0079 | 33 | 7.5 | $3.8 \pm 0.9 \pm 2.0$ |
| 16 | 0.375 | 0.0013 | 54 | 2.8 | $38.2 \pm 5.9 \pm 5.3$ |
| 16 | 0.375 | 0.0020 | 54 | 3.3 | $20.1 \pm 3.1 \pm 3.6$ |
| 16 | 0.375 | 0.0032 | 52 | 3.3 | $13.3 \pm 2.0 \pm 3.6$ |
| 16 | 0.375 | 0.0050 | 44 | 3.8 | $6.2 \pm 1.0 \pm 1.8$ |
| 16 | 0.65 | 0.00079 | 49 | 0 | $39.8 \pm 11.6 \pm 13.8$ |
| 16 | 0.65 | 0.0013 | 38 | 2.8 | $32.5 \pm 6.3 \pm 6.5$ |
| 16 | 0.65 | 0.0020 | 43 | 1.4 | $13.3 \pm 2.5 \pm 3.7$ |
| 16 | 0.65 | 0.0032 | 29 | 0 | $8.5 \pm 1.6 \pm 2.3$ |
| 28 | 0.175 | 0.0050 | 35 | 3.3 | $6.4 \pm 1.3 \pm 1.4$ |
| 28 | 0.175 | 0.0079 | 32 | 8.0 | $3.8 \pm 0.9 \pm 1.7$ |
| 28 | 0.375 | 0.0020 | 26 | 1.4 | $23.4 \pm 5.0 \pm 3.3$ |
| 28 | 0.375 | 0.0032 | 35 | 1.9 | $15.7 \pm 2.9 \pm 2.0$ |
| 28 | 0.375 | 0.0050 | 41 | 3.3 | $7.5 \pm 1.3 \pm 1.5$ |
| 28 | 0.375 | 0.0079 | 19 | 3.3 | $3.1 \pm 0.9 \pm 1.1$ |
| 28 | 0.65 | 0.0013 | 30 | 0.5 | $26.5 \pm 6.4 \pm 9.4$ |
| 28 | 0.65 | 0.0020 | 35 | 1.9 | $15.7 \pm 3.4 \pm 2.5$ |
| 28 | 0.65 | 0.0032 | 25 | 1.4 | $9.2 \pm 2.1 \pm 2.5$ |
| 28 | 0.65 | 0.0050 | 23 | 1.4 | $5.4 \pm 1.3 \pm 2.9$ |
| 63 | 0.375 | 0.0050 | 17 | 2.4 | $6.8 \pm 2.0 \pm 1.7$ |
| 63 | 0.375 | 0.0079 | 16 | 3.8 | $2.6 \pm 0.9 \pm 1.5$ |
| 63 | 0.65 | 0.0032 | 22 | 0.5 | $10.8 \pm 2.9 \pm 0.8$ |
| 63 | 0.65 | 0.0050 | 17 | 0.5 | $6.2 \pm 1.7 \pm 0.9$ |
| 63 | 0.65 | 0.0079 | 11 | 2.4 | $3.0 \pm 1.2 \pm 0.7$ |

Table 2: ZEUS 1993 $F_2^{D(3)}$ results. The overall normalisation uncertainty of 3.5% is not included. The data contain an estimated 15±10% fraction of double-dissociative events.
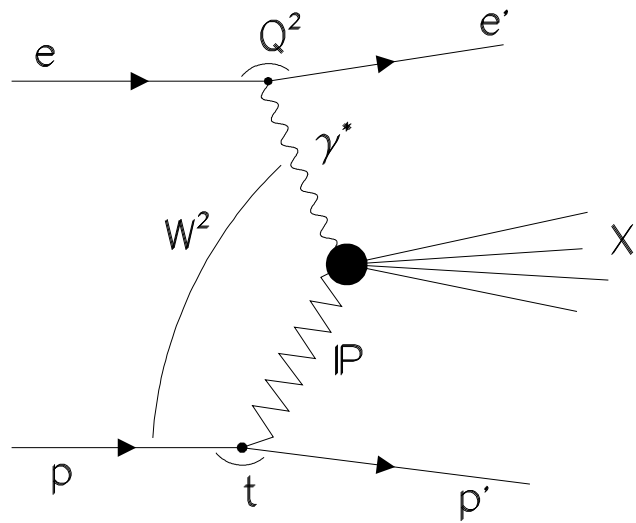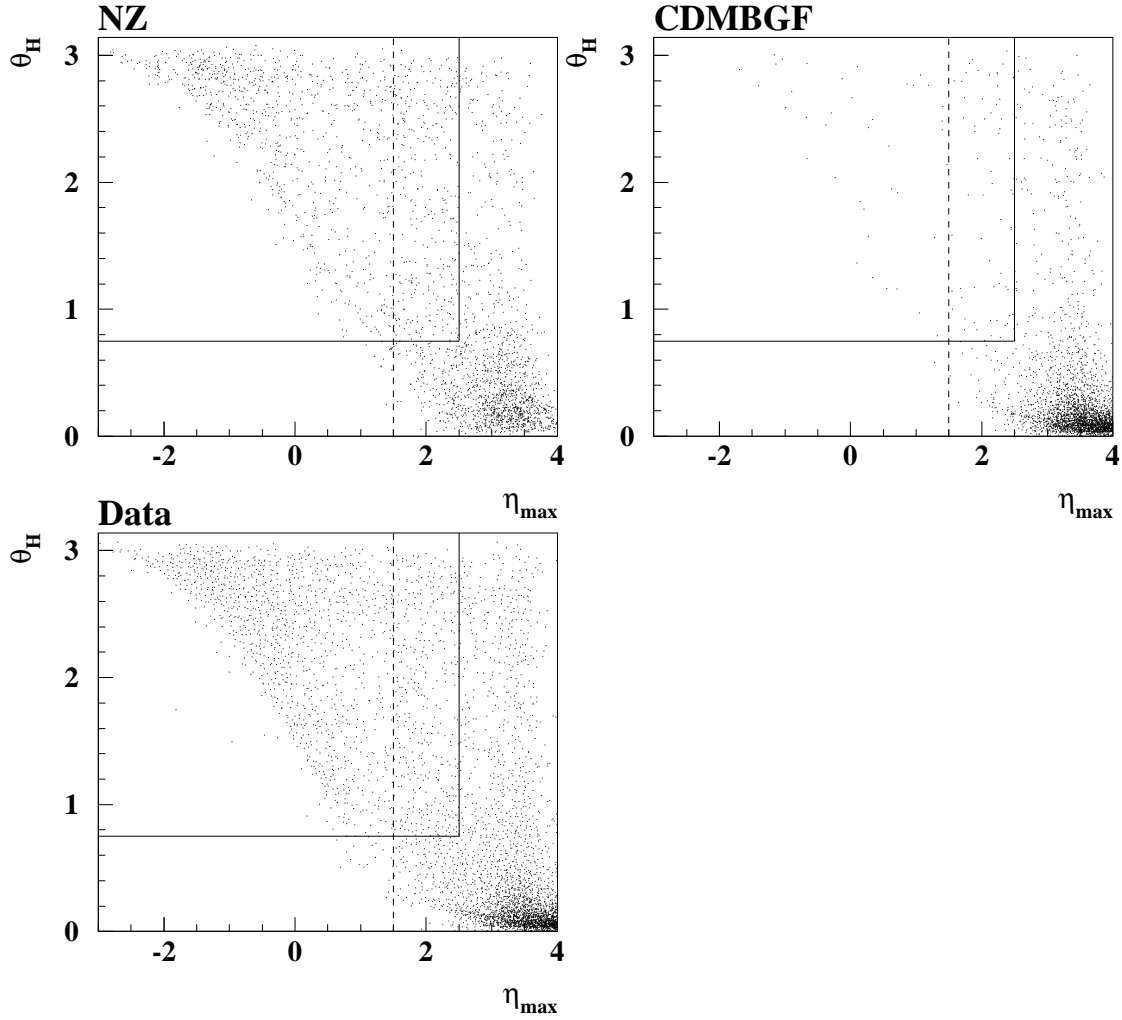
Figure 1: Diagram of a diffractive event.

Figure 2: $\theta_H$ versus $\eta_{max}$ distribution for diffractive (NZ) and non-diffractive (CDMBGF) Monte Carlo events and for the selected DIS data. The full line indicates the $\eta_{max}$-$\theta_H$ cut used to select diffractive events. The dotted line corresponds to $\eta_{max}$=1.5.
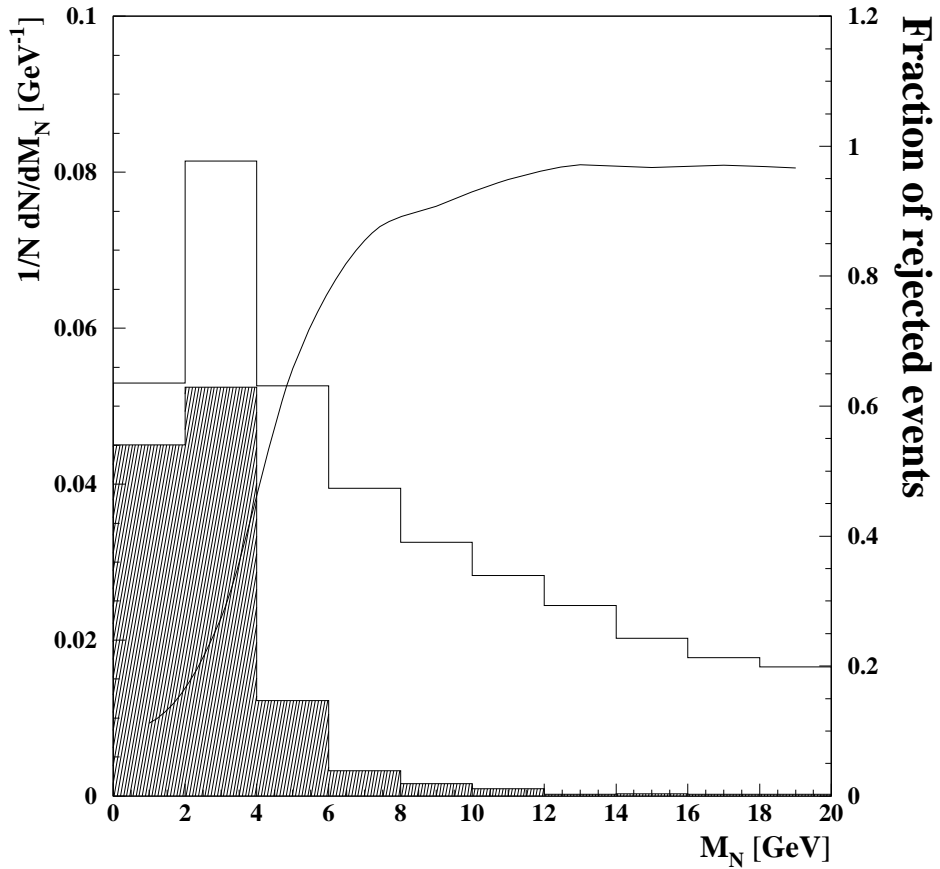
Figure 3: Acceptance for double dissociative events. The mass of the nucleon system, $M_N$, for double dissociative events generated by the PYTHIA Monte Carlo is indicated by the full line histogram. The shaded area indicates those events which are selected by the $\eta_{max}$-$\theta_H$ cut. The fraction of double dissociative events rejected by this cut, as a function of $M_N$, is indicated by the line.
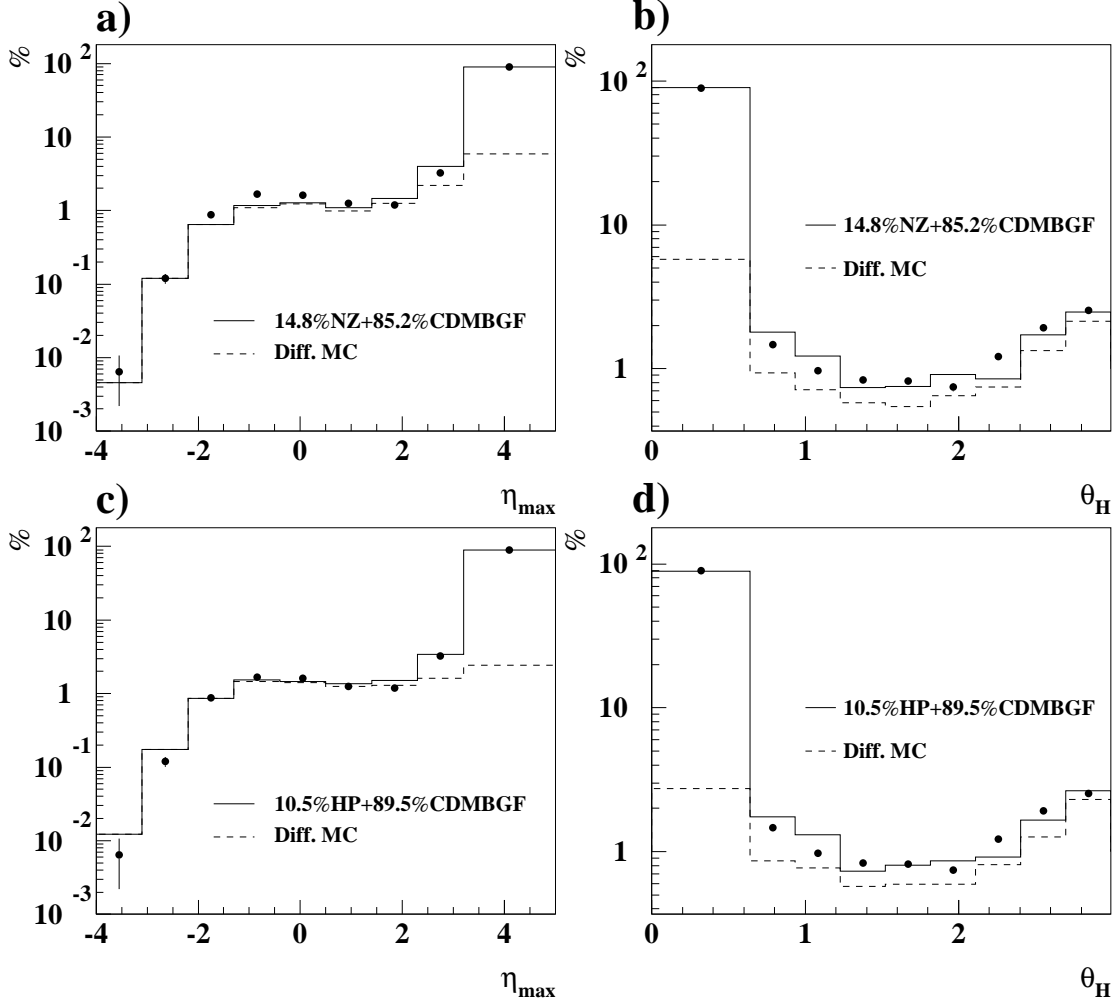
Figure 4: Percentage of DIS data as a function of $\eta_{\mathrm{max}}$ and $\theta_H$. The data are described by the sum of the diffractive and non-diffractive contributions obtained from Monte Carlo simulation, with relative fractions determined by a fit to the data. The dashed line corresponds to the diffractive contribution and the sum of the diffractive and non-diffractive Monte Carlo models is indicated by the full line.
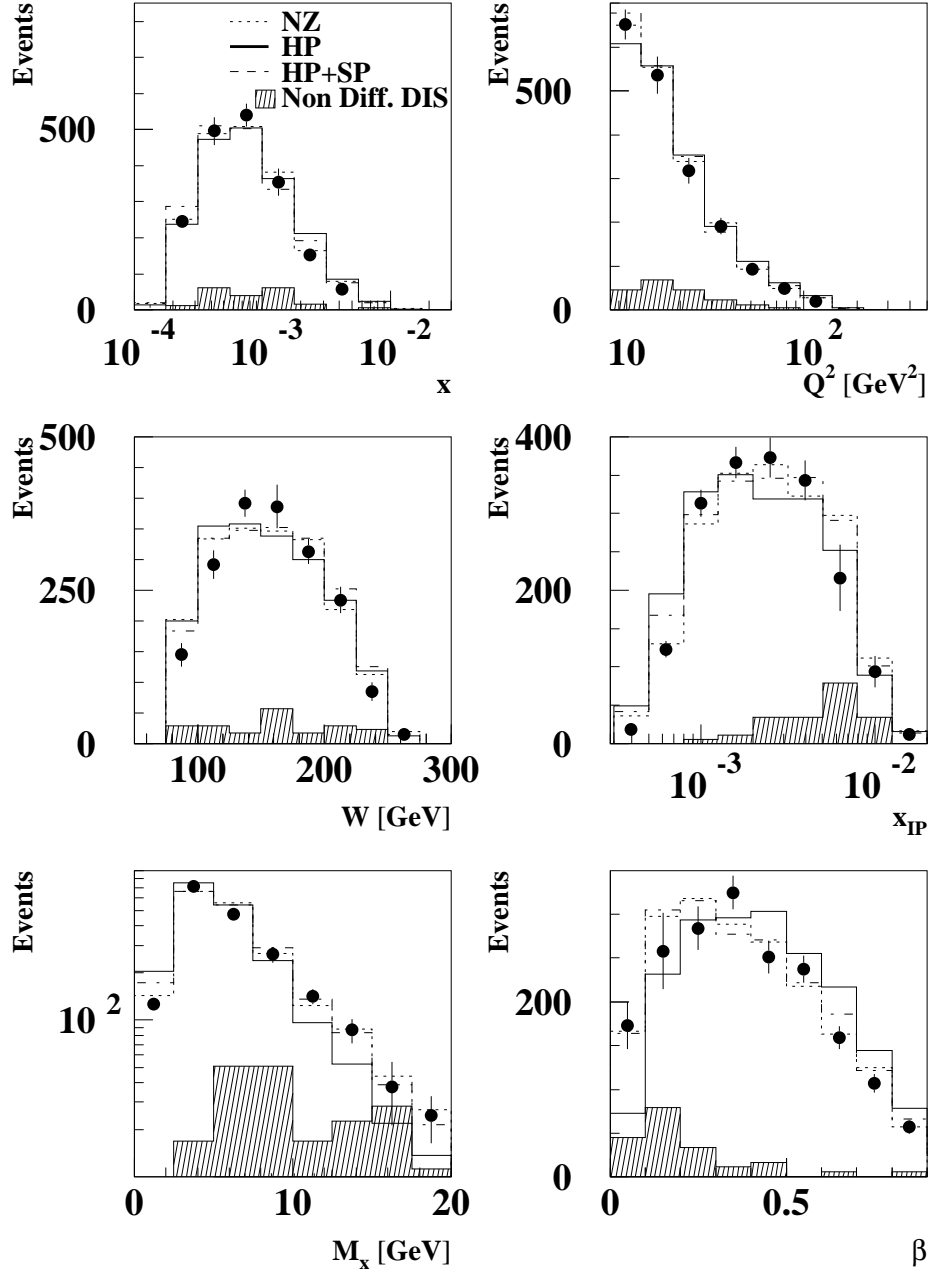
# ZEUS 1993



Figure 5: Observed distributions of $x$, $Q^2$, $W$, $x_{IP}$, $M_X$ and $\beta$ for the selected $(M_X, y)$ intervals. Uncorrected data are indicated by the dots. The errors are the statistical errors combined in quadrature with 50% of the non-diffractive DIS background. The predictions from HP (full line), HP+SP (dashed line) and NZ (dotted line) models are shown. The non-diffractive DIS background which has been subtracted from the data is indicated by the shaded area.
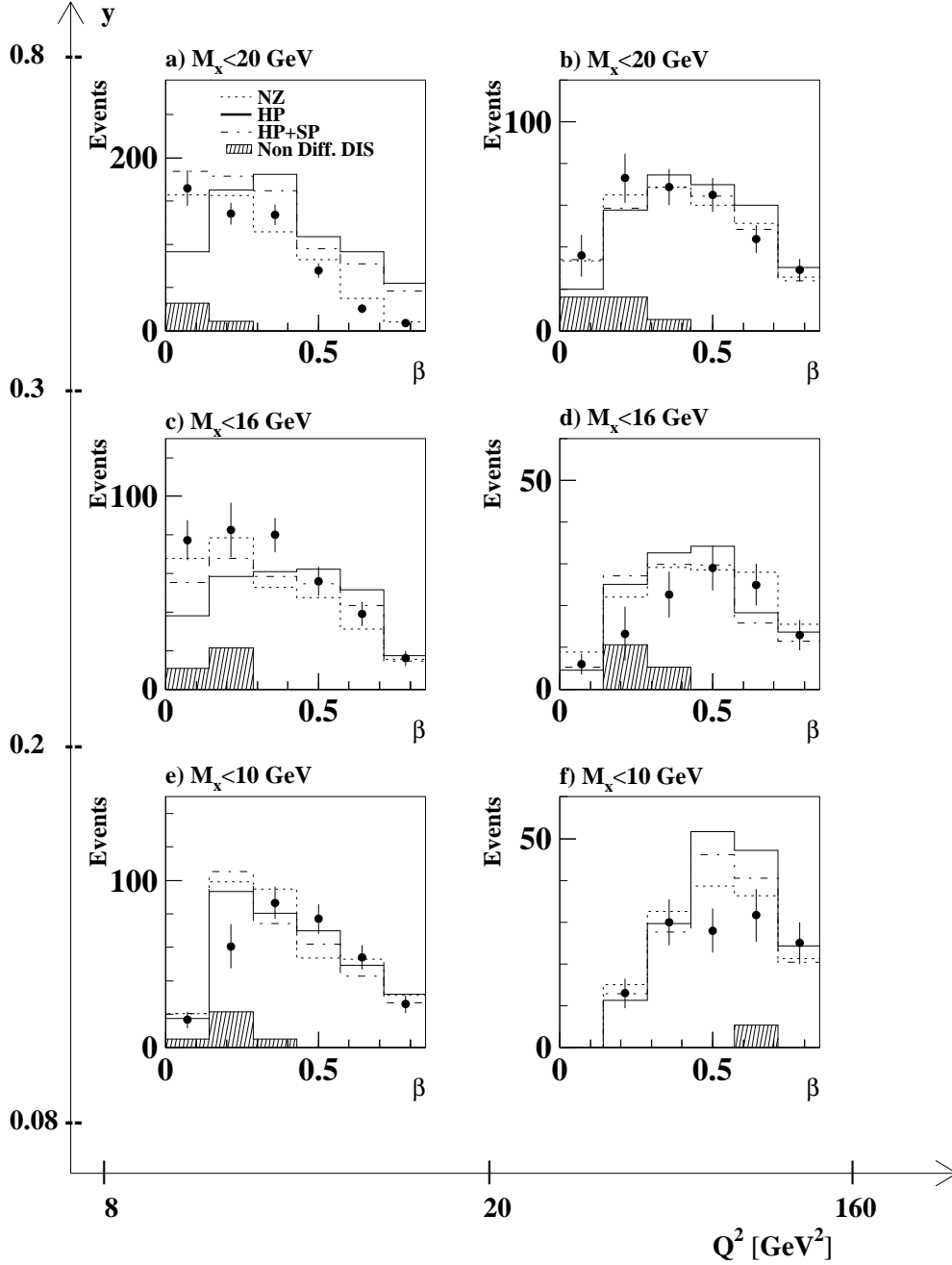
# ZEUS 1993



Figure 6: Observed $\beta$ distribution as a function of $(y, Q^2, M_X)$. The $Q^2$ intervals are 8-20 and 20-160 GeV$^2$, the $y$ intervals are 0.08-0.2, 0.2-0.3 and 0.3-0.8, and the $M_X$ intervals are (a,b) 0-20, (c,d) 0-16 and (e,f) 0-10 GeV. Uncorrected data are indicated by the dots. The errors are the statistical errors combined in quadrature with 50% of the non-diffractive DIS background. The predictions from HP (full line), HP+SP (dashed line) and NZ (dotted line) models are shown. The non-diffractive DIS background which has been subtracted from the data is indicated by the shaded area.
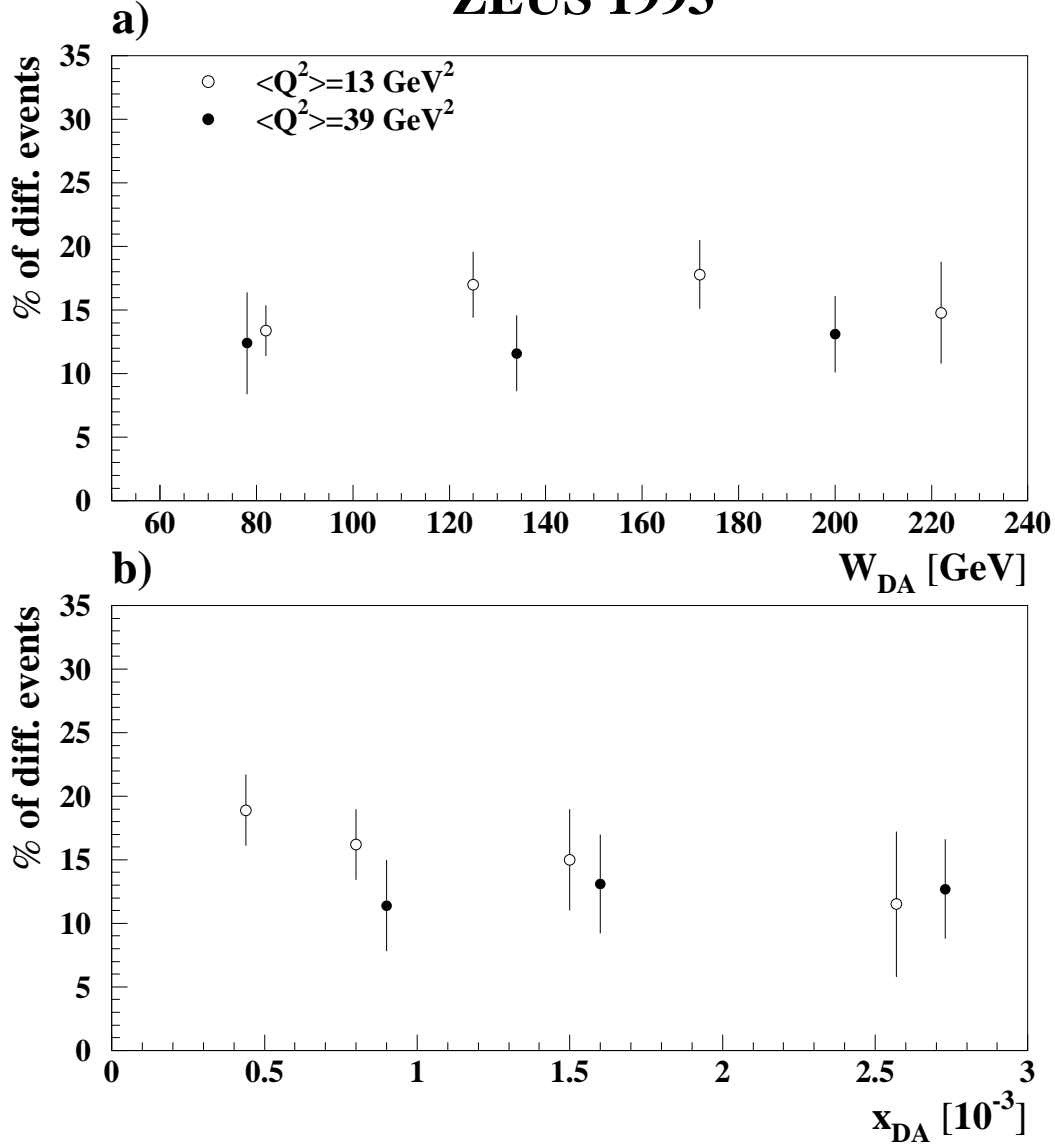
Figure 7: Observed fraction of diffractive events as a function of $W_{DA}$ and $x_{DA}$ in two $Q^2$ intervals. The data are fitted to the NZ model for diffractive processes and the CDMBGF model for the non-diffractive contribution. The errors are the statistical errors combined in quadrature with 50% of the non-diffractive DIS background.
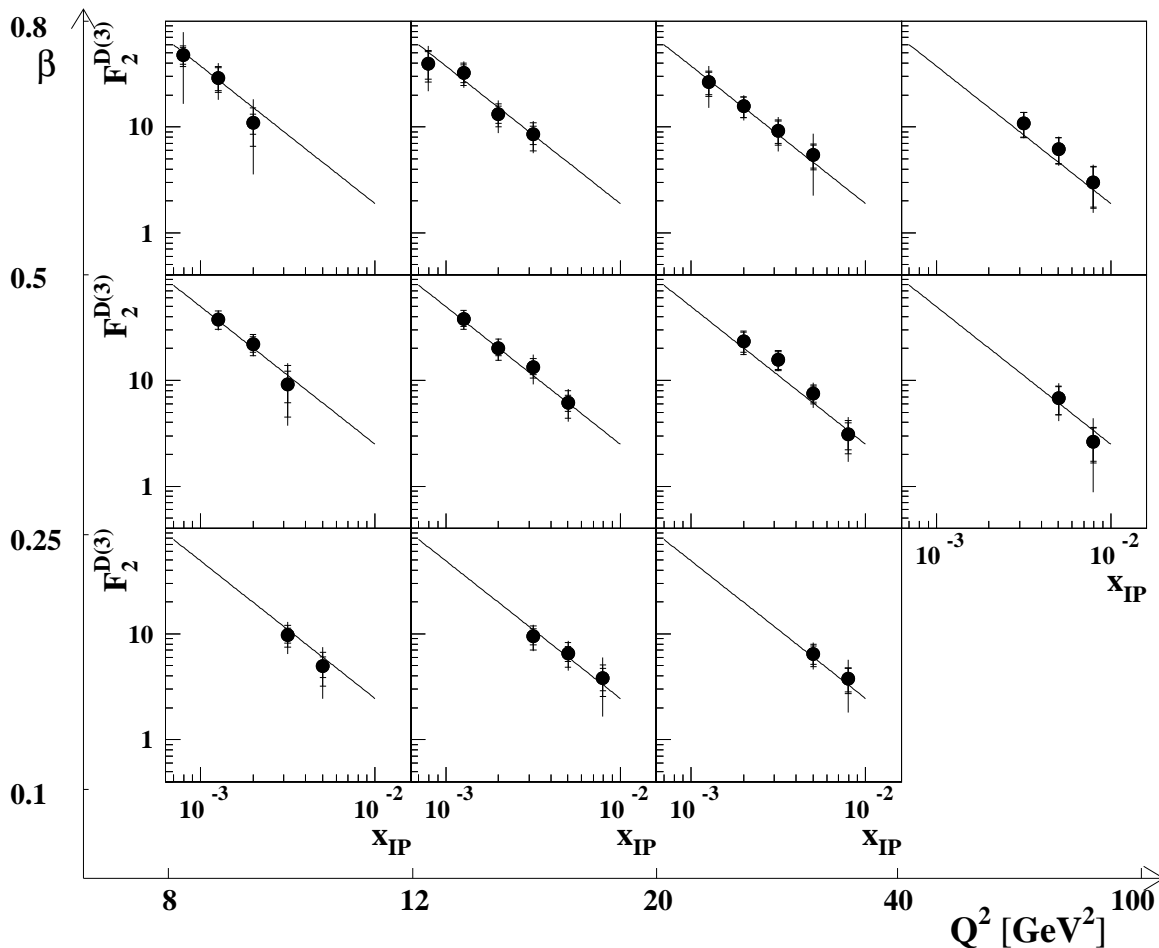
## ZEUS 1993



Figure 8: The results of $F_2^{D(3)}(\beta, Q^2, x_{I\!P})$ compared to the parametrisation discussed in the text. The inner error bars show the statistical errors, the outer bars correspond to the statistical and DIS event selection systematic errors added in quadrature, and the full line corresponds to the statistical and total systematic errors added in quadrature. Note that the data include an estimated 15% contribution due to double dissociation. The overall normalisation uncertainty of 3.5% due to the luminosity uncertainty is not included.
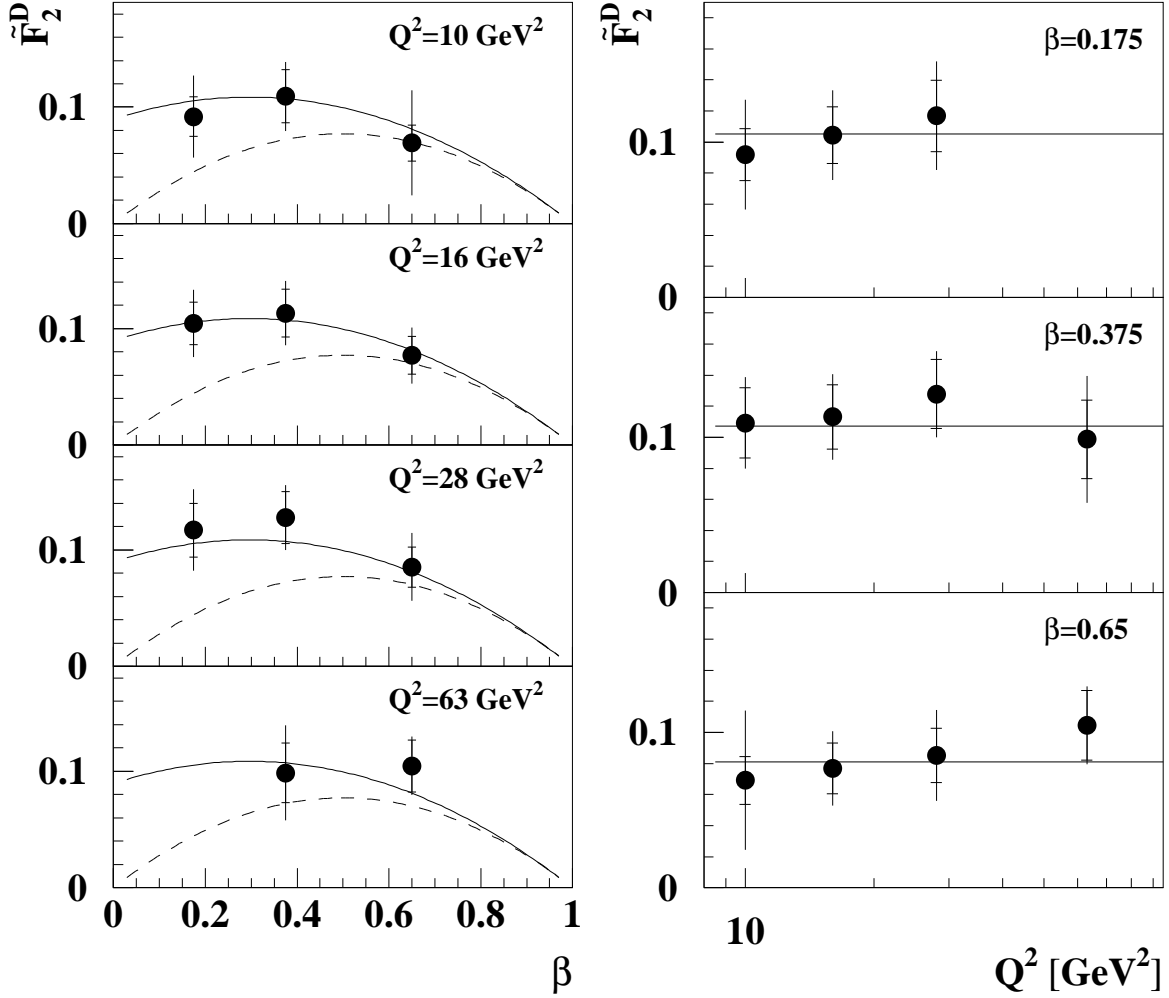
# ZEUS 1993



Figure 9: The results of $\tilde{F}_2^D(\beta, Q^2)$ compared to the parametrisation discussed in the text, indicated by the full line, and the $\beta(1-\beta)$ hard contribution, indicated by the dashed line. The inner error bars show the statistical errors, the outer bars correspond to the statistical and systematic errors added in quadrature. The systematic errors combine in quadrature the fits of the $x_{I\!P}$ dependence due to each of the systematic checks discussed in the text. Note that the overall normalisation is arbitrary and is determined by the experimental integration limits over $x_{I\!P}$ ($6.3 \cdot 10^{-4} < x_{I\!P} < 10^{-2}$). The data include an estimated 15% contribution due to double dissociation.
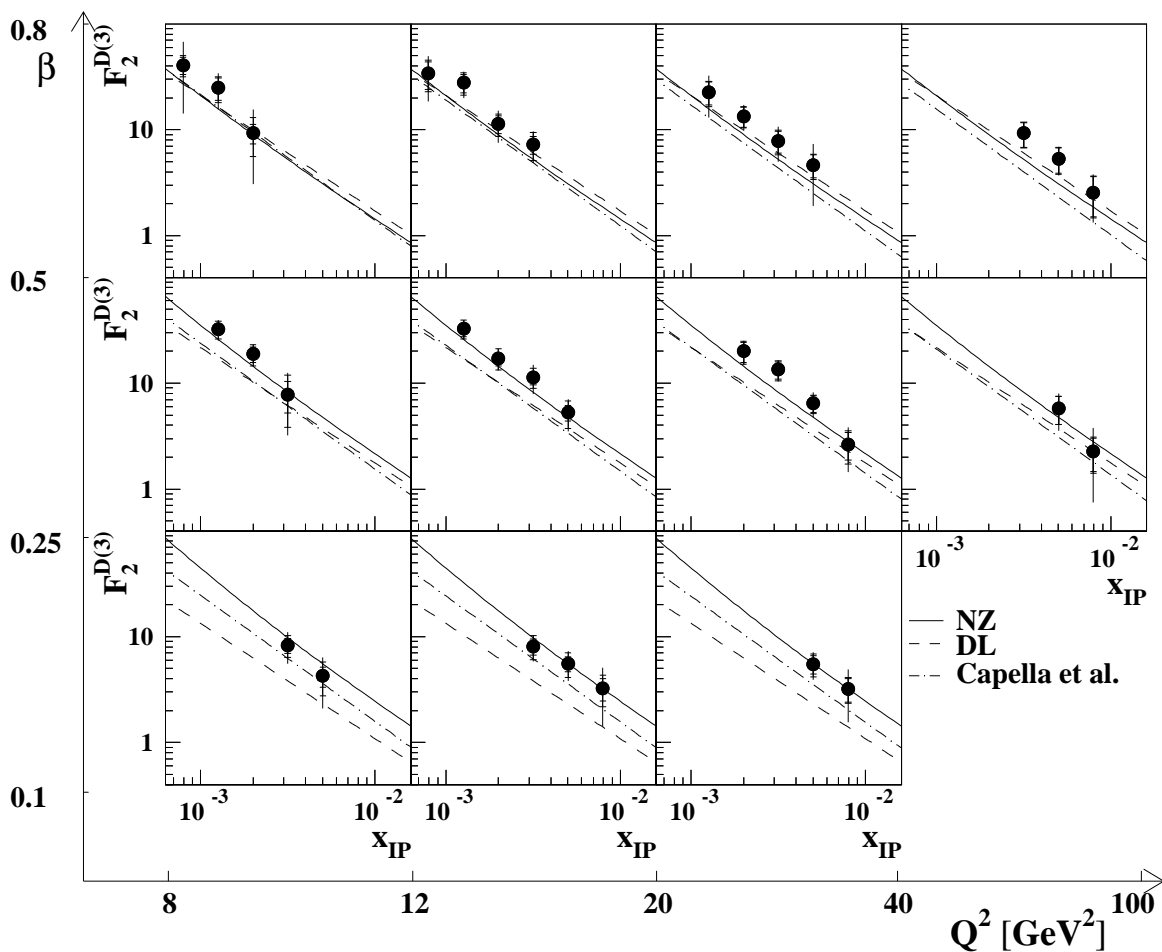
**ZEUS 1993**



Figure 10: The results of $F_2^{D(3)}$ compared to various models discussed in the text. Note that the estimated 15% contribution due to double dissociation has been subtracted in order to compare with models for the single dissociation cross section. The inner error bars show the statistical errors, the outer bars correspond to the statistical and DIS event selection systematic errors added in quadrature, and the full line corresponds to the statistical and total systematic errors added in quadrature. The overall normalisation uncertainty of 3.5% due to the luminosity and 10% due to the subtraction of the double dissociation background is not included.
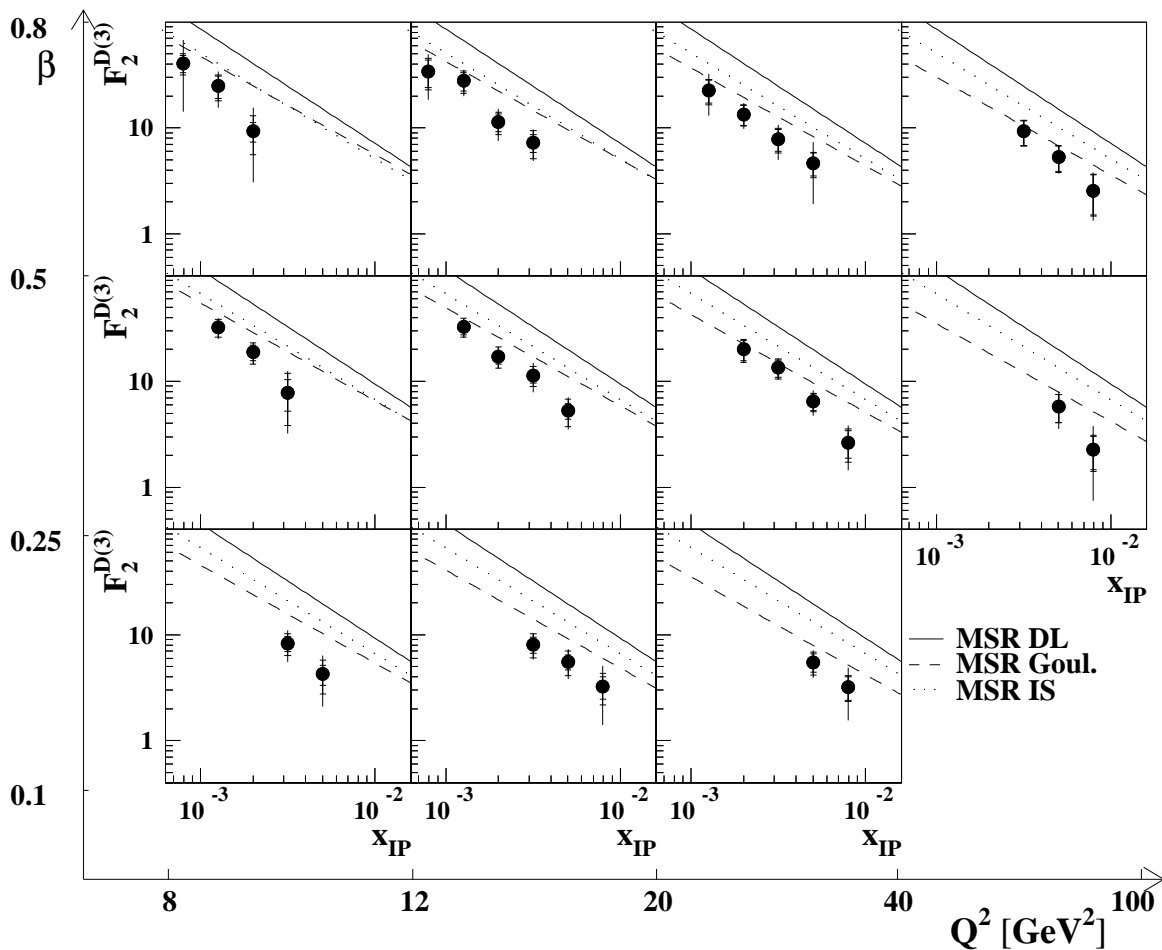
Figure 11: The results of $F_2^{D(3)}$ compared to an Ingelman-Schlein type model for which the momentum sum rule (MSR) for quarks within the pomeron is assumed. The $\beta$ dependence is taken from the parametrisation discussed in the text. Note that the estimated 15% contribution due to double dissociation has been subtracted in order to compare with models for the single dissociation cross section. The inner error bars show the statistical errors, the outer bars correspond to the statistical and DIS event selection systematic errors added in quadrature, and the full line corresponds to the statistical and total systematic errors added in quadrature. The overall normalisation uncertainty of 3.5% due to the luminosity and 10% due to the subtraction of the double dissociation background is not included.